

# Aqueous-phase mechanism for secondary organic aerosol formation from isoprene: application to the Southeast United States and co-benefit of SO<sub>2</sub> emission controls

E. A. Marais<sup>1</sup>, D. J. Jacob<sup>1,2</sup>, J. L. Jimenez<sup>3,4</sup>, P. Campuzano-Jost<sup>3,4</sup>, D. A. Day<sup>3,4</sup>, W. Hu<sup>3,4</sup>, J. Krechmer<sup>3,4</sup>, L. Zhu<sup>1</sup>, P. S. Kim<sup>2</sup>, C. C. Miller<sup>2</sup>, J. A. Fisher<sup>5</sup>, K. Travis<sup>1</sup>, K. Yu<sup>1</sup>, T. F. Hanisco<sup>6</sup>, G. M. Wolfe<sup>6,7</sup>, H. L. Arkinson<sup>8</sup>, H. O. T. Pye<sup>9</sup>, K. D. Froyd<sup>3,10</sup>, J. Liao<sup>3,10</sup>, V. F. McNeill<sup>11</sup>

<sup>1</sup>School of Engineering and Applied Sciences, Harvard University, Cambridge, MA, USA.

<sup>2</sup>Earth and Planetary Sciences, Harvard University, Cambridge, MA, USA.

<sup>3</sup>Cooperative Institute for Research in Environmental Sciences, University of Colorado, Boulder, CO, USA.

<sup>4</sup>Department of Chemistry and Biochemistry, University of Colorado, Boulder, CO, USA.

<sup>5</sup>School of Chemistry and School of Earth and Environmental Sciences, University of Wollongong, Wollongong, New South Wales, Australia.

<sup>6</sup>Atmospheric Chemistry and Dynamics Lab, NASA Goddard Space Flight Center, Greenbelt, MD, USA.

<sup>7</sup>Joint Center for Earth Systems Technology, University of Maryland Baltimore County, Baltimore, MD, USA.

<sup>8</sup>Department of Atmospheric and Oceanic Science, University of Maryland, College Park, MD, USA.

<sup>9</sup>National Exposure Research Laboratory, US EPA, Research Triangle Park, NC, USA.

<sup>10</sup>Chemical Sciences Division, Earth System Research Laboratory, NOAA, Boulder, Colorado, USA

<sup>11</sup>Department of Chemical Engineering, Columbia University, New York, New York 10027, USA.

## Abstract

Isoprene emitted by vegetation is an important precursor of secondary organic aerosol (SOA), but the mechanism and yields are uncertain. Aerosol is prevailingly aqueous under the humid conditions typical of isoprene-emitting regions. Here we develop an aqueous-phase mechanism for isoprene SOA formation coupled to a detailed gas-phase isoprene oxidation scheme. The mechanism is based on aerosol reactive uptake coefficients ( $\gamma$ ) for water-soluble isoprene oxidation products, including sensitivity to aerosol acidity and nucleophile concentrations. We apply this mechanism to simulation of aircraft (SEAC<sup>4</sup>RS) and ground-based (SOAS) observations over the Southeast US in summer 2013 using the GEOS-Chem chemical transport model. Emissions of nitrogen oxides ( $\text{NO}_x \equiv \text{NO} + \text{NO}_2$ ) over the Southeast US are such that the peroxy radicals produced from isoprene oxidation ( $\text{ISOPO}_2$ ) react significantly with both NO (high- $\text{NO}_x$  pathway) and  $\text{HO}_2$  (low- $\text{NO}_x$  pathway), leading to different suites of isoprene SOA precursors. We find a mean SOA mass yield of 3.3 % from isoprene oxidation, consistent with the observed relationship of total fine organic aerosol (OA) and formaldehyde (a product of isoprene oxidation). Isoprene SOA production is mainly contributed by two immediate gas-phase precursors, isoprene epoxydiols (IEPOX, 58% of isoprene SOA) from the low- $\text{NO}_x$  pathway and glyoxal (28%) from both low- and high- $\text{NO}_x$  pathways. This speciation is consistent with observations of IEPOX SOA from SOAS and SEAC<sup>4</sup>RS. Observations show a strong relationship between IEPOX SOA and sulfate aerosol that we explain as due to the effect of sulfate on aerosol acidity and volume. Isoprene SOA concentrations increase as  $\text{NO}_x$  emissions decrease (favoring the low- $\text{NO}_x$  pathway for isoprene oxidation), but decrease more

strongly as SO<sub>2</sub> emissions decrease (due to the effect of sulfate on aerosol acidity and volume). The US EPA projects 2013-2025 decreases in anthropogenic emissions of 34% for NO<sub>x</sub> (leading to 7% increase in isoprene SOA) and 48% for SO<sub>2</sub> (35% decrease in isoprene SOA). Reducing SO<sub>2</sub> emissions decreases sulfate and isoprene SOA by a similar magnitude, representing a factor of 2 co-benefit for PM<sub>2.5</sub> from SO<sub>2</sub> emission controls.

Keywords: isoprene, SOA yield, IEPOX, glyoxal, SEAC<sup>4</sup>RS, SOAS, formaldehyde.

Corresponding Author: emarais@seas.harvard.edu

## 1. Introduction

Isoprene emitted by vegetation is a major source of secondary organic aerosol (SOA) (Carlton et al., 2009, and references therein) with effects on human health, visibility, and climate. There is large uncertainty in the yield and composition of isoprene SOA (Scott et al., 2014; McNeill et al., 2014), involving a cascade of species produced in the gas-phase oxidation of isoprene and their interaction with pre-existing aerosol (Hallquist et al., 2009). We develop here a new aqueous-phase mechanism for isoprene SOA formation coupled to gas-phase chemistry, implement it in the GEOS-Chem chemical transport model (CTM) to simulate observations in the Southeast US, and from there derive new constraints on isoprene SOA yields and the contributing pathways.

Organic aerosol is ubiquitous in the atmosphere, often dominating fine aerosol mass (Zhang et al., 2007), including in the Southeast US where it accounts for more than 60% in summer (Attwood et al., 2014). It may be directly emitted by combustion as primary organic aerosol (POA), or produced within the atmosphere as SOA by oxidation of volatile organic compounds (VOCs). Isoprene ( $C_5H_8$ ) from vegetation is the dominant VOC emitted globally, and the Southeast US in summer is one of the largest isoprene-emitting regions in the world (Guenther et al., 2006). SOA yields from isoprene are low compared with larger VOCs (Pye et al., 2010), but isoprene emissions are much higher. Kim et al. (2015) estimated that isoprene accounts for 40% of total organic aerosol in the Southeast US in summer.

Formation of OA from oxidation of isoprene depends on local concentrations of nitrogen oxide radicals ( $NO_x \equiv NO + NO_2$ ) and pre-existing aerosol.  $NO_x$  concentrations determine the fate of organic peroxy radicals originating from isoprene oxidation ( $ISOPO_2$ ), leading to different cascades of oxidation products in the low- $NO_x$  and high- $NO_x$  pathways (Paulot et al.,

2009a; 2009b). Uptake of isoprene oxidation products to the aerosol phase depends on their vapor pressure (Donahue et al., 2006), solubility in aqueous media (Saxena and Hildeman, 1996), and subsequent condensed-phase reactions (Volkamer et al., 2007). Aqueous aerosol provides a medium for reactive uptake (Eddingsaas et al., 2010; Surratt et al., 2010) with dependences on acidity (Surratt et al., 2007a), concentration of nucleophiles such as sulfate (Surratt et al., 2007b), aerosol water (Carlton and Turpin, 2013), and organic coatings (Gaston et al., 2014).

We compile in Fig. 1 the published laboratory yields of isoprene SOA as a function of initial NO concentration and relative humidity (RH). Here and elsewhere, the isoprene SOA yield is defined as the mass of SOA produced per unit mass of isoprene oxidized. Isoprene SOA yields span a wide range, from <0.1% to >10%, with no systematic difference between low-NO<sub>x</sub> and high-NO<sub>x</sub> pathways. Yields tend to be higher in dry chambers (RH < 10%). Under such dry conditions isoprene SOA is expected to be solid (Virtanen et al., 2010; Song et al., 2015). At humid conditions more representative of the summertime boundary layer, aerosols are likely aqueous (Bateman et al., 2014). Standard isoprene SOA mechanisms used in atmospheric models assume reversible partitioning onto pre-existing organic aerosol, fitting the dry chamber data (Odum et al., 1996). However, this may not be appropriate for actual atmospheric conditions where aqueous-phase chemistry with irreversible reactive uptake of water-soluble gases is likely the dominant mechanism (Ervens et al., 2011; Carlton and Turpin, 2013). Several regional/global models have implemented mechanisms for aqueous-phase formation of isoprene SOA (Fu et al., 2008, 2009; Carlton et al., 2008; Myriokefalitakis et al., 2011; Liu et al., 2012; Pye et al., 2013; Lin et al., 2014).

Here we present a mechanism for irreversible aqueous-phase isoprene SOA formation integrated within a detailed chemical mechanism for isoprene gas-phase oxidation, thus linking isoprene SOA formation to gas-phase chemistry and avoiding more generic volatility-based parameterizations that assume dry organic aerosol (Odum et al., 1996; Donahue et al., 2006). We use this mechanism in the GEOS-Chem CTM to simulate observations from the SOAS (surface) and SEAC<sup>4</sup>RS (aircraft) field campaigns over the Southeast US in summer 2013, with focus on isoprene SOA components and on the relationship between OA and formaldehyde (HCHO). HCHO is a high-yield oxidation product of isoprene (Palmer et al., 2003) and we use the OA-HCHO relationship as a constraint on isoprene SOA yields. SOAS measurements were made at a ground site in rural Centreville, Alabama (Hu et al., 2015; <http://soas2013.rutgers.edu/>). SEAC<sup>4</sup>RS measurements were made from the NASA DC-8 aircraft with extensive boundary layer coverage across the Southeast (Toon et al., 2016; SEAC<sup>4</sup>RS Archive).

## **2. Chemical mechanism for isoprene SOA formation**

The default treatment of isoprene SOA in GEOS-Chem at the time of this work (v9-02; <http://geos-chem.org>) followed a standard parameterization operating independently from the gas-phase chemistry mechanism and based on reversible partitioning onto pre-existing OA of generic semivolatile products of isoprene oxidation by OH and NO<sub>3</sub> radicals (Pye et al., 2010). Here we implement a new mechanism for reactive uptake by aqueous aerosols of species produced in the isoprene oxidation cascade of the GEOS-Chem gas-phase mechanism. This couples SOA formation to the gas-phase chemistry and is in accord with increased evidence for a major role of aqueous aerosols in isoprene SOA formation (Ervens et al., 2011).

The standard gas-phase isoprene oxidation mechanism in GEOS-Chem v9-02 is described in Mao et al. (2013) and is based on best knowledge at the time building on mechanisms for the oxidation of isoprene by OH (Paulot et al., 2009a; 2009b) and NO<sub>3</sub> (Rollins et al., 2009). Updates implemented in this work are described below and in companion papers applying GEOS-Chem to simulation of observed gas-phase isoprene oxidation products over the Southeast US in summer 2013 (Fisher et al., 2016; Travis et al., 2016). Most gas-phase products of the isoprene oxidation cascade in GEOS-Chem have high dry deposition velocity, competing in some cases with removal by oxidation and aerosol formation (Nguyen et al., 2015a; Travis et al., 2016).

Figure 2 shows the isoprene oxidation cascade in GEOS-Chem leading to SOA formation. Reaction pathways leading to isoprene SOA precursors are described below. Yields are in mass percent, unless stated otherwise. Reactive ISOPO<sub>2</sub> isomers formed in the first OH oxidation step react with NO, the hydroperoxyl radical (HO<sub>2</sub>), other peroxy radicals (RO<sub>2</sub>), or undergo isomerization (Peeters et al., 2009). The NO reaction pathway (high-NO<sub>x</sub> pathway) yields C<sub>5</sub> hydroxy carbonyls, methyl vinyl ketone, methacrolein, and first-generation isoprene nitrates (ISOPN). The first three products go on to produce glyoxal and methylglyoxal, which serve as SOA precursors. The overall yield of glyoxal from the high-NO<sub>x</sub> pathway is 7 mol % (yield on a molar basis). Oxidation of ISOPN by OH and O<sub>3</sub> is as described by Lee et al. (2014). Reaction of ISOPN with OH produces saturated dihydroxy dinitrates (DHDN), 21 and 27 mol % from the beta and delta channels respectively (Lee et al., 2014), and 10 mol % isoprene epoxydiols (IEPOX) from each channel (Jacobs et al., 2014). We also adopt the mechanism of Lin et al. (2013) to generate C<sub>4</sub> hydroxyepoxides (methacrylic acid epoxide and hydroxymethylmethyl- $\alpha$ -lactone, both denoted MEPOX) from OH oxidation of a

peroxyacylnitrate formed when methacrolein reacts with OH followed by NO<sub>2</sub>. Only hydroxymethylmethyl- $\alpha$ -lactone is shown in Fig. 2.

The HO<sub>2</sub> reaction pathway for ISOPO<sub>2</sub> leads to formation of hydroxyhydroperoxides (ISOPOOH) that are oxidized to IEPOX (Paulot et al., 2009b) and several low-volatility products, represented here as C<sub>5</sub>-LVOC (Krechmer et al., 2015). The kinetics of IEPOX oxidation by OH is uncertain, and experimentally determined IEPOX lifetimes vary from 8 to 28 h for an OH concentration of  $1 \times 10^6$  molecules cm<sup>-3</sup> (Jacobs et al., 2013; Bates et al., 2014). In GEOS-Chem we apply the fast kinetics of Jacobs et al. (2013) and reduce the yield of IEPOX from ISOPOOH from 100 to 75%, within the range observed by St. Clair et al. (2016), to address a factor of 4 overestimate in simulated IEPOX pointed out by Nguyen et al. (2015a). The IEPOX discrepancy could alternatively be addressed with an order-of-magnitude increase in uptake by aerosol (see below) but the model would then greatly overestimate the observed IEPOX SOA concentrations in SOAS and SEAC<sup>4</sup>RS (Section 4).

IEPOX oxidizes to form glyoxal and methylglyoxal (Bates et al., 2014). The overall glyoxal yield from the ISOPO<sub>2</sub> + HO<sub>2</sub> pathway is 6 mol %. Krechmer et al. (2015) report a 2.5 mol % yield of C<sub>5</sub>-LVOC from ISOPOOH but we reduce this to 0.5 mol % to reproduce surface observations of the corresponding aerosol products (Section 4). Methyl vinyl ketone and methacrolein yields from the ISOPO<sub>2</sub> + HO<sub>2</sub> pathway are 2.5 and 3.8 mol %, respectively (Liu et al., 2013), sufficiently low that they do not lead to significant SOA formation.

Minor channels for ISOPO<sub>2</sub> are isomerization and reaction with RO<sub>2</sub>. Isomerization forms hydroperoxyaldehydes (HPALD) that go on to photolyze, but products are uncertain (Peeters and Müller, 2010). We assume 25 mol % yield each of glyoxal and methylglyoxal from HPALD photolysis in GEOS-Chem following Stavrakou et al. (2010). Reaction of ISOPO<sub>2</sub> with

RO<sub>2</sub> leads to the same suite of C<sub>4</sub>-C<sub>5</sub> carbonyls as reaction with NO (C<sub>5</sub> hydroxy carbonyls, methacrolein, and methyl vinyl ketone) and from there to glyoxal and methylglyoxal.

Immediate aerosol precursors from the isoprene + OH oxidation cascade are identified in Fig. 2. For the high-NO<sub>x</sub> pathway (ISOPO<sub>2</sub> + NO channel) these include glyoxal and methylglyoxal (McNeill et al., 2012), ISOPN (Darer et al., 2011; Hu et al., 2011), DHDN (Lee et al., 2014), MEPOX (Lin et al., 2013), and IEPOX (Jacobs et al., 2014). For the low-NO<sub>x</sub> pathway (ISOPO<sub>2</sub> + HO<sub>2</sub> channel) aerosol precursors are IEPOX (Eddingsaas et al., 2010), C<sub>5</sub>-LVOC (Krechmer et al., 2015, in which the aerosol-phase species is denoted ISOPOOH-SOA), glyoxal, and methylglyoxal. Glyoxal and methylglyoxal are also produced from the ISOPO<sub>2</sub> + RO<sub>2</sub> and ISOPO<sub>2</sub> isomerization channels.

Ozonolysis and oxidation by NO<sub>3</sub> are additional minor isoprene reaction pathways (Fig. 2). The NO<sub>3</sub> oxidation pathway is a potentially important source of isoprene SOA at night (Brown et al., 2009) from the irreversible uptake of low-volatility second-generation hydroxynitrates (NT-ISOPN) (Ng et al., 2008; Rollins et al., 2009). We update the gas-phase chemistry of Rollins et al. (2009) as implemented by Mao et al. (2013) to include formation of 4 mol % of the aerosol-phase precursor NT-ISOPN from first-generation alkyl nitrates (Rollins et al., 2009). Ozonolysis products are volatile and observed SOA yields in chamber studies are low (< 1%; Kleindienst et al., 2007). In GEOS-Chem only methylglyoxal is an aerosol precursor from isoprene ozonolysis.

We implement uptake of isoprene oxidation products to aqueous aerosols using laboratory-derived reactive uptake coefficients ( $\gamma$ ) as given by Anttila et al. (2006) and Gaston et al. (2014):



$$\gamma = \left[ \frac{1}{\alpha} + \frac{3\omega}{4rRTH^*k_{aq}} \right]^{-1} \quad (1).$$

Here  $\alpha$  is the mass accommodation coefficient (taken as 0.1 for all immediate SOA precursors in Fig. 2),  $\omega$  is the mean gas-phase molecular speed ( $\text{cm s}^{-1}$ ),  $r$  is the aqueous particle radius (cm),  $R$  is the universal gas constant ( $0.08206 \text{ L atm K}^{-1} \text{ mol}^{-1}$ ),  $T$  is temperature (K),  $H^*$  is the effective Henry's Law constant ( $\text{M atm}^{-1}$ ) accounting for any fast dissociation equilibria in the aqueous phase, and  $k_{aq}$  is the pseudo first-order aqueous-phase reaction rate constant ( $\text{s}^{-1}$ ) for conversion to non-volatile products.

Precursors with epoxide functionality, IEPOX and MEPOX, undergo acid-catalyzed epoxide ring opening and nucleophilic addition in the aqueous phase. The aqueous-phase rate constant formulation is from Eddingsaas et al. (2010),

$$k_{aq} = k_{H^+} [H^+] + k_{nuc} [nuc] [H^+] + k_{HSO_4^-} [HSO_4^-] \quad (2),$$

and includes three channels: acid-catalyzed ring opening followed by nucleophilic addition of  $\text{H}_2\text{O}$  ( $k_{H^+}$  in  $\text{M}^{-1} \text{ s}^{-1}$ ) leading to methyltetrols, acid-catalyzed ring opening followed by nucleophilic addition of sulfate and nitrate ions ( $nuc \equiv \text{SO}_4^{2-} + \text{NO}_3^-$ ,  $k_{nuc}$  in  $\text{M}^{-2} \text{ s}^{-1}$ ) leading to organosulfates and organonitrates, and concerted protonation and nucleophilic addition by bisulfate,  $\text{HSO}_4^-$  ( $k_{HSO_4^-}$  in  $\text{M}^{-1} \text{ s}^{-1}$ ), leading to organosulfates.

Precursors with nitrate functionality ( $-\text{ONO}_2$ ), ISOPN and DHDN, hydrolyze to form low-volatility polyols and nitric acid (Hu et al., 2011; Jacobs et al., 2014), so  $k_{aq}$  in Eq. (1) is the hydrolysis rate constant.

Glyoxal and methylglyoxal form SOA irreversibly by surface uptake followed by aqueous-phase oxidation and oligomerization to yield non-volatile products (Liggio et al., 2005; Volkamer et al., 2009; Nozière et al., 2009; Ervens et al., 2011; Knote et al., 2014). Glyoxal forms SOA with higher yields during the day than at night due to OH aqueous-phase chemistry (Tan et al., 2009; Volkamer et al., 2009; Summer et al., 2014). We use a daytime  $\gamma$  of  $2.9 \times 10^{-3}$  for glyoxal from Liggio et al. (2005) and a nighttime  $\gamma$  of  $5 \times 10^{-6}$  (Waxman et al., 2013; Sumner et al., 2014). The SOA yield of methylglyoxal is small compared with that of glyoxal (McNeill et al., 2012). A previous GEOS-Chem study by Fu et al. (2008) used the same  $\gamma$  ( $2.9 \times 10^{-3}$ ) for glyoxal and methylglyoxal. Reaction rate constants are similar for aqueous-phase processing of glyoxal and methylglyoxal (Buxton et al., 1997; Ervens et al., 2003), but  $H^*$  of glyoxal is about 4 orders of magnitude higher. Here we scale the  $\gamma$  for methylglyoxal to the ratio of effective Henry's law constants:  $H^* = 3.7 \times 10^3 \text{ M atm}^{-1}$  for methylglyoxal (Tan et al., 2010) and  $H^* = 2.7 \times 10^7 \text{ M atm}^{-1}$  for glyoxal (Sumner et al., 2014). The resulting uptake of methylglyoxal is very slow and makes a negligible contribution to isoprene SOA.

The species  $\text{C}_5$ -LVOC from ISOPOOH oxidation and NT-ISOPN from isoprene reaction with  $\text{NO}_3$  have very low volatility and are assumed to condense to aerosols with a  $\gamma$  of 0.1 limited by mass accommodation. Results are insensitive to the precise value of  $\gamma$  since uptake by aerosols is the main sink for these species in any case.

Table 1 gives input variables used to calculate  $\gamma$  for IEPOX, ISOPN, and DHDN by Eqs. (1) and (2). Rate constants are from experiments in concentrated media, representative of aqueous aerosols, so no activity correction factors are applied. Reported experimental values of  $k_{H^+}$  vary by an order of magnitude from  $1.2 \times 10^{-3} \text{ M}^{-1} \text{ s}^{-1}$  (Eddingsaas et al., 2010) to  $3.6 \times 10^{-2} \text{ M}^{-1} \text{ s}^{-1}$  (Cole-Filipiak et al., 2010). Values of  $k_{nuc}$  vary by 3 orders of magnitude from  $2 \times 10^{-4} \text{ M}^{-1} \text{ s}^{-1}$

$^2 \text{ s}^{-1}$  (Eddingsaas et al., 2010) to  $5.2 \times 10^{-1} \text{ M}^{-2} \text{ s}^{-1}$  (Piletic et al., 2013). Reported values of IEPOX  $H^*$  vary by two orders of magnitude (Eddingsaas et al., 2010; Nguyen et al., 2014). We chose values of  $k_{H^+}$ ,  $k_{nuc}$ , and  $H^*$  to fit the SOAS and SEAC<sup>4</sup>RS observations of total IEPOX SOA and IEPOX organosulfates, as discussed in Section 4.

Table 2 lists average values of  $\gamma$  for all immediate aerosol precursors in the Southeast US boundary layer in summer as simulated by GEOS-Chem (Section 3).  $\gamma$  for IEPOX is a strong function of pH and increases from  $1 \times 10^{-4}$  to  $1 \times 10^{-2}$  as pH decreases from 3 to 0. Gaston et al. (2014) reported order-of-magnitude higher values of  $\gamma$  for IEPOX, reflecting their use of a higher  $H^*$ , but this would lead in our model to an overestimate of IEPOX SOA observations (Section 4).

The value of  $\gamma$  for MEPOX is assumed to be 30 times lower than that of IEPOX when the aerosol is acidic ( $\text{pH} < 4$ ), due to slower acid-catalyzed ring opening (Piletic et al., 2013; Riedel et al., 2015). At  $\text{pH} > 4$  we assume that  $\gamma$  for IEPOX and MEPOX are the same (Riedel et al., 2015), but they are then very low.

Isoprene SOA formation in clouds is not considered here. Acid-catalyzed pathways would be slow. Observations show that the isoprene SOA yield in the presence of laboratory-generated clouds is low (0.2-0.4%; Brégonzio-Rozier et al., 2015). Wagner et al. (2015) found no significant production of SOA in boundary layer clouds over the Southeast US during SEAC<sup>4</sup>RS.

### 3. GEOS-Chem simulation and isoprene SOA yields

Several companion papers apply GEOS-Chem to interpret SEAC<sup>4</sup>RS and surface data over the Southeast US in summer 2013 including Kim et al. (2015) for aerosols, Fisher et al. (2016) for organic nitrates, Travis et al. (2016) for ozone and  $\text{NO}_x$ , and Zhu et al. (2016) for HCHO. These studies use a model version with  $0.25^\circ \times 0.3125^\circ$  horizontal resolution over North

America, nested within a  $4^{\circ} \times 5^{\circ}$  global simulation. Here we use a  $2^{\circ} \times 2.5^{\circ}$  global GEOS-Chem simulation with no nesting. Yu et al. (2016) found little difference between  $0.25^{\circ} \times 0.3125^{\circ}$  and  $2^{\circ} \times 2.5^{\circ}$  resolutions in simulated regional statistics for isoprene chemistry.

The reader is referred to Kim et al. (2015) for a general presentation of the model, the treatment of aerosol sources and sinks, and evaluation with Southeast US aerosol observations; and to Travis et al. (2016) and Fisher et al. (2016) for presentation of gas-phase chemistry and comparisons with observed gas-phase isoprene oxidation products. Isoprene emission is from the MEGAN v2.1 inventory (Guenther et al., 2012). The companion papers decrease isoprene emission by 15% from the MEGAN v2.1 values to fit the HCHO data (Zhu et al., 2016), but this is not applied here.

Our SOA simulation differs from that of Kim et al. (2015). They assumed fixed 3% and 10% mass yields of SOA from isoprene and monoterpenes, respectively, and parameterized SOA formation from anthropogenic and open fire sources as a kinetic irreversible process following Hodzic and Jimenez (2011). Here we use our new aqueous-phase mechanism for isoprene SOA coupled to gas-phase chemistry as described in Section 2, and otherwise use the semivolatile reversible partitioning scheme of Pye et al. (2010) for monoterpene, anthropogenic, and open fire SOA. Kim et al. (2015) found no systematic bias in detailed comparisons to OA measurements from SEAC<sup>4</sup>RS and from surface networks. We find a low bias, as shown below, because the reversible partitioning scheme yields low anthropogenic and open fire SOA concentrations.

Organic aerosol and sulfate contribute most of the aerosol mass over the Southeast US in summer, while nitrate is negligibly small (Kim et al., 2015). GEOS-Chem uses the ISORROPIA thermodynamic model (Fountoukis and Nenes, 2007) to simulate sulfate-nitrate-ammonium (SNA) aerosol composition, water content, and acidity as a function of local conditions.

Simulated aerosol pH along the SEAC<sup>4</sup>RS flight tracks in the Southeast US boundary layer averages 1.3 (interquartiles 0.92 and 1.8). The aerosol pH remains below 3 even when sulfate aerosol is fully neutralized by ammonia (Guo et al., 2015).

We consider that the aqueous aerosol population where isoprene SOA formation can take place is defined by the sulfate aerosol population. This assumes that all aqueous aerosol particles contain some sulfate, and that all sulfate is aqueous. Clear-sky RH measured from the aircraft in the Southeast US boundary layer during SEAC<sup>4</sup>RS averaged  $72 \pm 17\%$ , and the corresponding values in GEOS-Chem sampled along the flight tracks averaged  $66 \pm 16\%$ . These RHs are sufficiently high that sulfate aerosol can reliably be expected to be aqueous (Wang et al., 2008). The rate of gas uptake by the sulfate aerosol is computed with the pseudo-first order reaction rate constant  $k_{het}$  ( $s^{-1}$ ) (Schwartz, 1986; Jacob, 2000):

$$k_{het} = \int_0^\infty 4\pi r^2 \left( \frac{r}{D_g} + \frac{4}{\gamma\omega} \right)^{-1} n(r) dr \quad (3),$$

where  $D_g$  is the gas-phase diffusion constant (taken to be  $0.1 \text{ cm}^2 \text{ s}^{-1}$ ) and  $n(r)$  is the number size distribution of sulfate aerosol ( $\text{cm}^{-4}$ ). The first and second terms in parentheses describe the limitations to gas uptake from gas-phase diffusion and aqueous-phase reaction, respectively.

The sulfate aerosol size distribution including RH-dependent hygroscopic growth factors is from the Global Aerosol Data Set (GADS) of Koepke et al. (1997), as originally implemented in GEOS-Chem by Martin et al. (2003) and updated by Drury et al. (2010). The GADS size distribution compares well with observations over the eastern US in summer (Drury et al., 2010), including for SEAC<sup>4</sup>RS (Kim et al., 2015). We compute  $n(r)$  locally in GEOS-Chem by taking

the dry SNA mass concentration, converting from mass to volume with a dry aerosol mass density of  $1700 \text{ kg m}^{-3}$  (Hess et al., 1998), applying the aerosol volume to the dry sulfate size distribution in GADS, and then applying the GADS hygroscopic growth factors. We verified that the hygroscopic growth factors from GADS agree within 10% with those computed locally from ISORROPIA.

Figure 2 shows the mean branching ratios for isoprene oxidation in the Southeast US boundary layer as calculated by GEOS-Chem. 87% of isoprene reacts with OH, 8% with ozone, and 5% with  $\text{NO}_3$ . Oxidation of isoprene by OH produces  $\text{ISOPO}_2$  of which 51% reacts with NO (high- $\text{NO}_x$  pathway), 35% reacts with  $\text{HO}_2$ , 8% isomerizes, and 6% reacts with other  $\text{RO}_2$  radicals.

Glyoxal is an aerosol precursor common to all isoprene + OH pathways in our mechanism with yields of 7 mol % from the  $\text{ISOPO}_2 + \text{NO}$  pathway, 6 mol % from  $\text{ISOPO}_2 + \text{HO}_2$ , 11 mol % from  $\text{ISOPO}_2 + \text{RO}_2$ , and 25 mol % from  $\text{ISOPO}_2$  isomerization. For the Southeast US conditions we thus find that 44% of glyoxal is from the  $\text{ISOPO}_2 + \text{NO}$  pathway, 24% from  $\text{ISOPO}_2 + \text{HO}_2$ , 8% from  $\text{ISOPO}_2 + \text{RO}_2$ , and 24% from  $\text{ISOPO}_2$  isomerization.

The mean total yield of isoprene SOA computed in GEOS-Chem for the Southeast US boundary layer is 3.3%, as shown in Fig. 2. IEPOX contributes 1.9% and glyoxal 0.9%. The low- $\text{NO}_x$  pathway involving  $\text{ISOPO}_2$  reaction with  $\text{HO}_2$  contributes 73% of the total isoprene SOA yield, mostly from IEPOX, even though this pathway is only 35% of the fate of  $\text{ISOPO}_2$ . The high- $\text{NO}_x$  pathway contributes 16% of isoprene SOA, mostly from glyoxal. MEPOX contribution to isoprene SOA is small (2%) and consistent with a recent laboratory study that finds low SOA yields from this pathway under humid conditions (Nguyen et al., 2015b). The minor low- $\text{NO}_x$  pathways from  $\text{ISOPO}_2$  isomerization and reaction with  $\text{RO}_2$  contribute 8% of

isoprene SOA through glyoxal. The remainder of isoprene SOA formation (3%) is from nighttime oxidation by  $\text{NO}_3$ .

The dominance of IEPOX and glyoxal as precursors for isoprene SOA was previously found by McNeill et al. (2012) using a photochemical box model. Both IEPOX and glyoxal are produced photochemically, and both are removed photochemically in the gas phase by reaction with OH (and photolysis for glyoxal). The mean lifetimes of IEPOX and glyoxal against gas-phase photochemical loss average 1.6 and 2.3 h respectively for SEAC<sup>4</sup>RS daytime conditions; mean lifetimes against reactive uptake by aerosol are 31 and 20 hours, respectively. For both species, aerosol uptake is thus a minor sink competing with gas-phase photochemical loss.

Although we have assumed here the fast gas-phase kinetics from Jacobs et al. (2013) for the IEPOX + OH reaction, this result would not change if we used the slower kinetics from Bates et al. (2014).

The dominance of gas-phase loss over aerosol uptake for both IEPOX and glyoxal implies that isoprene SOA formation is highly sensitive to their reactive uptake coefficients  $\gamma$  and to the aqueous aerosol mass concentration (in both cases,  $\gamma$  is small enough that uptake is controlled by bulk aqueous-phase rather than surface reactions). We find under SEAC<sup>4</sup>RS conditions that  $\gamma$  for IEPOX is mainly controlled by the  $\text{H}^+$  concentration ( $k_{\text{H}^+}[\text{H}^+]$  in Eq. (2)), with little contribution from nucleophile-driven and  $\text{HSO}_4^-$ -driven channels, although this is based on highly uncertain rate constants (Section 2). Consistency with SOAS and SEAC<sup>4</sup>RS observations will be discussed below.

The 3.3% mean yield of isoprene SOA from our mechanism is consistent with the fixed yield of 3% assumed by Kim et al. (2015) in their GEOS-Chem simulation of the SEAC<sup>4</sup>RS period, including extensive comparisons to OA observations that showed a 40% mean

contribution of isoprene to total OA. We conducted a sensitivity simulation using the default isoprene SOA mechanism in GEOS-Chem based on reversible partitioning of semivolatile oxidation products onto pre-existing OA (Pye et al., 2010). The isoprene SOA yield in that simulation was only 1.1%. The observed correlation of OA with HCHO in SEAC<sup>4</sup>RS supports our higher yield, as shown below.

#### 4. Observational constraints on isoprene SOA yields

Isoprene is the largest source of HCHO in the Southeast US (Millet et al., 2006), and we use the observed relationship between OA and HCHO to evaluate the GEOS-Chem isoprene SOA yields. The SEAC<sup>4</sup>RS aircraft payload included measurements of OA from an Aerodyne Aerosol Mass Spectrometer (HR-ToF-AMS; DeCarlo et al, 2006; Canagaratna et al, 2007) concurrent with HCHO from a laser-induced fluorescence instrument (ISAF; Cazorla et al., 2015). Column HCHO was also measured during SEAC<sup>4</sup>RS from the OMI satellite instrument (González Abad et al., 2015; Zhu et al., 2016), providing a proxy for isoprene emission (Palmer et al., 2003; 2006).

Figure 3 (left) shows the observed and simulated relationships between OA and HCHO mixing ratios in the boundary layer. There is a strong correlation in the observations and in the model ( $R = 0.79$  and  $R = 0.82$ , respectively). OA simulated with our aqueous-phase isoprene SOA mechanism reproduces the observed slope ( $2.8 \pm 0.3 \mu\text{g sm}^{-3} \text{ ppbv}^{-1}$ , vs.  $3.0 \pm 0.4 \mu\text{g sm}^{-3} \text{ ppbv}^{-1}$  in the observations). Similarly strong correlations and consistency between model and observations are found with column HCHO measured from OMI (Fig. 3, right). The estimated error on individual OMI HCHO observations is about 30% (Millet et al., 2006).



Also shown in Fig. 3 is a sensitivity simulation with the default GEOS-Chem mechanism based on reversible partitioning with pre-existing organic aerosol (Pye et al., 2010) and producing a 1.1% mean isoprene SOA yield, as compared to 3.3% in our simulation with the aqueous-phase mechanism. That sensitivity simulation shows the same OA-HCHO correlation ( $R = 0.82$ ) but underestimates the slope ( $2.0 \pm 0.3 \mu\text{g sm}^{-3} \text{ ppbv}^{-1}$ ). The factor of 3 increase in our isoprene SOA yield does not induce a proportional increase in the slope, as isoprene contributes only  $\sim 40\%$  of OA in the Southeast US. But the slope is sensitive to the isoprene SOA yield, and the good agreement between our simulation and observations supports our estimate of a mean 3.3% yield for the Southeast US.

Figure 3 shows an offset between the model and observations illustrated by the regression lines. We overestimate HCHO by 0.4 ppbv on average because we did not apply the 15% downward correction to MEGAN v2.1 isoprene emissions (Zhu et al., 2016). We also underestimate total OA measured by the AMS in the boundary layer by  $1.1 \mu\text{g sm}^{-3}$  (mean AMS OA is  $5.8 \pm 4.3 \mu\text{g sm}^{-3}$ ; model OA is  $4.7 \pm 4.4 \mu\text{g sm}^{-3}$ ). The bias can be explained by our omission of anthropogenic and open fire SOA, found by Kim et al. (2015) to account on average for 18% of OA in SEAC<sup>4</sup>RS.

Figure 4 shows time series of the isoprene SOA components IEPOX SOA and C<sub>5</sub>-LVOC SOA at Centreville, Alabama during SOAS. AMS observations from Hu et al. (2015) and Krechmer et al. (2015) are compared to model values. IEPOX SOA and C<sub>5</sub>-LVOC SOA are on average 17% and 2% of total AMS OA, respectively (Hu et al., 2015; Krechmer et al., 2015). The model reproduces mean IEPOX SOA and C<sub>5</sub>-LVOC SOA without bias, supporting the conclusion that IEPOX is the dominant contributor to isoprene SOA in the Southeast US (Fig. 2).

Figure 5 shows the relationships of daily mean IEPOX SOA and sulfate concentrations at Centreville and in the SEAC<sup>4</sup>RS boundary layer. The same factor analysis method was used to derive IEPOX SOA in SEAC<sup>4</sup>RS as in SOAS, however the uncertainty is larger for the aircraft observations due to the much wider range of conditions encountered. There is a strong correlation between IEPOX SOA and sulfate, both in observations and the model, with similar slopes. Correlation between IEPOX SOA and sulfate has similarly been observed at numerous Southeast US monitoring sites (Budisulistiorini et al., 2013; 2015; Xu et al., 2015; Hu et al., 2015). Xu et al. (2015) concluded that IEPOX SOA may form by nucleophilic addition of sulfate (sulfate channels in Eq. (2)) leading to organosulfates. However, we find in our model that the H<sup>+</sup>-catalyzed channel ( $k_{H^+}[H^+]$  term in Eq. (2)) contributes 90% of IEPOX SOA formation throughout the Southeast US boundary layer, and that sulfate channels play only a minor role. The correlation of IEPOX SOA and sulfate in the model is because increasing sulfate drives an increase in aqueous aerosol volume and acidity. Although dominance of the H<sup>+</sup>-catalyzed channel is sensitive to uncertainties in the rate constants (Section 2), measurements from the PALMS laser mass spectrometer during SEAC<sup>4</sup>RS (Liao et al., 2015) show a mean IEPOX organosulfate concentration of  $0.13 \mu\text{g sm}^{-3}$ , amounting to at most 9% of total IEPOX SOA. The organosulfate should be a marker of the sulfate channels because its hydrolysis is negligibly slow (Hu et al., 2011).

Correlation between IEPOX SOA and sulfate is also apparent in the spatial distribution of IEPOX SOA, as observed by the SEAC<sup>4</sup>RS aircraft below 2 km and simulated by GEOS-Chem along the aircraft flight tracks (Fig. 6). The correlation between simulated and observed IEPOX SOA in Fig. 6 is  $R = 0.70$ . Average (mean) IEPOX SOA is  $1.4 \pm 1.4 \mu\text{g sm}^{-3}$  in the observations and  $1.3 \pm 1.2 \mu\text{g sm}^{-3}$  in the model. The correlation between IEPOX SOA and sulfate is 0.66 in

the observations and 0.77 in the model. IEPOX SOA concentrations are highest in the industrial Midwest and Kentucky, and in Louisiana-Mississippi, coincident with the highest sulfate concentrations sampled on the flights. We also see in Fig. 6 frequent observations of very low IEPOX SOA (less than  $0.4 \mu\text{g sm}^{-3}$ ) that are well captured by the model. These are associated with very low sulfate (less than  $1 \mu\text{g sm}^{-3}$ ).

The mean IEPOX SOA concentration simulated by the model for the SEAC<sup>4</sup>RS period (background contours in Fig. 6) is far more uniform than IEPOX SOA simulated along the flight tracks. This shows the importance of day-to-day variations in sulfate in driving IEPOX SOA variability. IEPOX SOA contributed on average 24% of total OA in the SEAC<sup>4</sup>RS observations, and 28% in GEOS-Chem sampled along the flight tracks and as a regional mean. With IEPOX SOA accounting for 58% of isoprene SOA in the model (Fig. 2), this amounts to a 41-48% contribution of isoprene to total OA, consistent with the previous estimate of 40% by Kim et al. (2015).

## 5. Effect of Anthropogenic Emission Reductions

The EPA projects that US anthropogenic emissions of  $\text{NO}_x$  and  $\text{SO}_2$  will decrease respectively by 34% and 48% from 2013 to 2025 (EPA, 2014). We conducted a GEOS-Chem sensitivity simulation to examine the effect of these changes on isoprene SOA, assuming no other changes and further assuming that the emission decreases are uniform across the US.

Figure 7 shows the individual and combined effects of  $\text{NO}_x$  and  $\text{SO}_2$  emission reductions on the branching pathways for isoprene oxidation, sulfate mass concentration, aerosol pH, and isoprene SOA in the Southeast US boundary layer in summer. Reducing  $\text{NO}_x$  emission by 34% decreases the mean NO concentration by only 23%, in part because decreasing OH increases the

NO<sub>x</sub> lifetime and in part because decreasing ozone increases the NO/NO<sub>2</sub> ratio. There is no change in HO<sub>2</sub>. We find a 10% decrease in the high-NO<sub>x</sub> pathway and a 6% increase in the low-NO<sub>x</sub> pathway involving ISOPO<sub>2</sub> + HO<sub>2</sub>. Aerosol sulfate decreases by 2% and there is no change in [H<sup>+</sup>]. The net effect is a 7% increase in isoprene SOA, as the major individual components IEPOX SOA and glyoxal SOA increase by 17% and decrease by 8%, respectively.

A 48% decrease in SO<sub>2</sub> emissions drives a 36% reduction in sulfate mass concentration, leading to a decline in aerosol volume (31%) that reduces uptake of all isoprene SOA precursors. The decrease in aerosol [H<sup>+</sup>] (26%) further reduces IEPOX uptake. Decline in aerosol volume and [H<sup>+</sup>] have a comparable effect on IEPOX SOA, as the change in each due to SO<sub>2</sub> emission reductions is similar (~30%) and uptake of IEPOX SOA is proportional to the product of the two (Section 4). IEPOX SOA and glyoxal SOA decrease by 45% and 26%, respectively, and total isoprene SOA decreases by 35%. Pye et al. (2013) included uptake of IEPOX to aqueous aerosols in a regional chemical transport model and similarly found that SO<sub>2</sub> emissions are more effective than NO<sub>x</sub> emissions at reducing IEPOX SOA in the Southeast US. Remarkably, we find that reducing SO<sub>2</sub> emissions decreases sulfate and isoprene SOA with similar effectiveness (Fig. 7). With sulfate contributing ~30% of present-day PM<sub>2.5</sub> in the Southeast US and isoprene SOA contributing ~25% (Kim et al., 2015), this represents a factor of 2 co-benefit on PM<sub>2.5</sub> from reducing SO<sub>2</sub> emissions.

## 6. Conclusions

Standard mechanisms for formation of isoprene secondary organic aerosol (SOA) in chemical transport models assume reversible partitioning of isoprene oxidation products to pre-existing dry OA. This may be appropriate for dry conditions in experimental chambers but not

for typical atmospheric conditions where the aerosol is mostly aqueous. Here we developed an aqueous-phase reactive uptake mechanism coupled to a detailed gas-phase isoprene chemistry mechanism to describe the reactive uptake of water-soluble isoprene oxidation products to aqueous aerosol. We applied this mechanism in the GEOS-Chem chemical transport model to simulate surface (SOAS) and aircraft (SEAC<sup>4</sup>RS) observations over the Southeast US in summer 2013.

Our mechanism includes different channels for isoprene SOA formation by the high-NO<sub>x</sub> pathway, when the isoprene peroxy radicals (ISOPO<sub>2</sub>) react with NO, and in the low-NO<sub>x</sub> pathway where they react mostly with HO<sub>2</sub>. The main SOA precursors are found to be isoprene epoxide (IEPOX) in the low-NO<sub>x</sub> pathway and glyoxal in the high- and low-NO<sub>x</sub> pathways. Both of these precursors have dominant gas-phase photochemical sinks, and so their uptake by aqueous aerosol is nearly proportional to the reactive uptake coefficient  $\gamma$  and to the aqueous aerosol mass concentration. The  $\gamma$  for IEPOX is mostly determined by the rate of H<sup>+</sup>-catalyzed ring opening in the aqueous phase.

Application of our mechanism to the Southeast US indicates a mean isoprene SOA yield of 3.3% on a mass basis. By contrast, a conventional mechanism based on reversible uptake of semivolatile isoprene oxidation products yields only 1.1%. Simulation of the observed relationship of OA with formaldehyde (HCHO) provides support for our higher yield. We find that the low-NO<sub>x</sub> pathway is 5 times more efficient than the high-NO<sub>x</sub> pathway for isoprene SOA production. Under Southeast US conditions, IEPOX and glyoxal account respectively for 58% and 28% of isoprene SOA.

Our model simulates well the observations and variability of IEPOX SOA at the surface and from aircraft. The observations show a strong correlation with sulfate that we reproduce in

the model. We find this is due to the effect of sulfate on aerosol pH and volume concentration, increasing IEPOX uptake by the  $H^+$ -catalyzed ring-opening mechanism. Low concentrations of sulfate are associated with very low IEPOX SOA, both in the observations and the model, and we attribute this to the compounding effects of low sulfate on aerosol  $[H^+]$  and on aerosol volume.

The US EPA has projected that US  $NO_x$  and  $SO_2$  emissions will decrease by 34 and 48% respectively from 2013 to 2025. We find in our model that the  $NO_x$  reduction will increase isoprene SOA by 7%, reflecting greater importance of the low- $NO_x$  pathway. The  $SO_2$  reduction will decrease isoprene SOA by 35%, due to decreases in both aerosol  $[H^+]$  and volume concentration. The combined effect of these two changes is to decrease isoprene SOA by 32%, corresponding to a decrease in the isoprene SOA mass yield from 3.3% to 2.3%. Decreasing  $SO_2$  emissions by 48% has similar relative effects on sulfate (36%) and isoprene SOA (35%). Considering that sulfate presently accounts for about 30% of  $PM_{2.5}$  in the Southeast US in summer, while isoprene SOA contributes 25%, we conclude that decreasing isoprene SOA represents a factor of 2 co-benefit when reducing  $SO_2$  emissions.

## Acknowledgements

We are grateful to the entire NASA SEAC<sup>4</sup>RS team for their help in the field, in particular Paul Wennberg, John Crounse, Jason St. Clair, and Alex Teng for their CIT-CIMS measurements. Thanks also to Jesse Kroll for assisting in the interpretation of chamber study results. This work was funded by the NASA Tropospheric Chemistry Program, the NASA Air Quality Applied Sciences Team, and a South African National Research Foundation Fellowship and Schlumberger Faculty for the Future Fellowship to EAM. WH, JEK, PCJ, DAD, and JLJ

505 were supported by NASA NNX12AC03G/NNX15AT96G and NSF AGS-1243354. JEK was  
506 supported by EPA STAR (FP-91770901-0) and CIRES Fellowships. JAF acknowledges support  
507 from a University of Wollongong Vice Chancellor's Postdoctoral Fellowship. HCHO  
508 observations were acquired with support from NASA ROSES SEAC<sup>4</sup>RS grant  
509 NNH10ZDA001N. Although this document has been reviewed by U.S. EPA and approved for  
510 publication, it does not necessarily reflect U.S. EPA's policies or views.

511

## 512 References

- 513 Anttila, T., Kiendler-Scharr, A., Tillmann, R., and Mentel, T. F.: On the reactive uptake of  
514 gaseous compounds by organic-coated aqueous aerosols: Theoretical analysis and  
515 application to the heterogeneous hydrolysis of N<sub>2</sub>O<sub>5</sub>, *J. Phys. Chem. A*, 110, 10435-10443,  
516 doi:10.1021/jp062403c, 2006.
- 517 Attwood, A. R., Washenfelder, R. A., Brock, C. A., Hu, W., Baumann, K., Campuzano-Jost, P.,  
518 Day, D. A., Edgerton, E. S., Murphy, D. M., Palm, B. B., McComiskey, A., Wagner, N. L.,  
519 de Sá, S. S., Ortega, A., Martin, S. T., Jimenez, J. L., and Brown, S. S.: Trends in sulfate  
520 and organic aerosol mass in the Southeast U.S.: Impact on aerosol optical depth and  
521 radiative forcing, *Geophys. Res. Lett.*, 41, 7701-7709, doi:10.1002/2014gl061669, 2014.
- 522 Bateman, A. P., Bertram, A. K., and Martin, S. T.: Hygroscopic influence on the semisolid-to-  
523 liquid transition of secondary organic materials, *J. Phys. Chem. A*, 119, 4386-4395,  
524 doi:10.1021/jp508521c, 2014.
- 525 Bates, K. H., Crounse, J. D., St Clair, J. M., Bennett, N. B., Nguyen, T. B., Seinfeld, J. H., Stoltz,  
526 B. M., and Wennberg, P. O.: Gas phase production and loss of isoprene epoxydiols, *J.*  
527 *Phys. Chem. A*, 118, 1237-1246, doi:10.1021/jp4107958, 2014.
- 528 Brégonzio-Rozier, L., Giorio, C., Siekmann, F., Pangui, E., Morales, S. B., Temime-Roussel, B.,  
529 Gratien, A., Michoud, V., Cazaunau, M., DeWitt, H. L., Tapparo, A., Monod, A.,  
530 and Doussin, J.-F.: Secondary organic aerosol formation from isoprene photooxidation  
531 during cloud condensation–evaporation cycles, *Atmos. Chem. Phys. Discuss.*, 15, 20561-  
532 20596, doi:10.5194/acpd-15-20561-2015, 2015.
- 533 Brown, S. S., De Gouw, J. A., Warneke, C., Ryerson, T. B., Dubé, W. P., Atlas, E., Weber, R. J.,  
534 Peltier, R. E., Neuman, J. A., Roberts, J. M., Swanson, A., Flocke, F., McKeen, S. A.,  
535 Brioude, J., Sommariva, R., Trainer, M., Fehsenfeld, F. C., and Ravishankara, A. R.:  
536 Nocturnal isoprene oxidation over the Northeast United States in summer and its impact on  
537 reactive nitrogen partitioning and secondary organic aerosol, *Atmos. Chem. Phys.*, 9, 3027-  
538 3042, doi:10.5194/acp-9-3027-2009, 2009.
- 539 Budisulistiorini, S. H., Canagaratna, M. R., Croteau, P. L., Marth, W. J., Baumann, K., Edgerton,  
540 E. S., Shaw, S. L., Knipping, E. M., Worsnop, D. R., Jayne, J. T., Gold, A., and Surratt, J.  
541 D.: Real-time continuous characterization of secondary organic aerosol derived from  
542 isoprene epoxydiols in downtown Atlanta, Georgia, using the Aerodyne aerosol chemical  
543 speciation monitor, *Environ. Sci. Technol.*, 47, 5686-5694, doi:10.1021/es400023n, 2013.
- 544 Budisulistiorini, S. H., Li, X., Bairai, S. T., Renfro, J., Liu, Y., Liu, Y. J., McKinney, K. A.,  
545 Martin, S. T., McNeill, V. F., Pye, H. O. T., Nenes, A., Neff, M. E., Stone, E. A., Mueller,  
546 S., Knote, C., Shaw, S. L., Zhang, Z., Gold, A., and Surratt, J. D.: Examining the effects of  
547 anthropogenic emissions on isoprene-derived secondary organic aerosol formation during  
548 the 2013 Southern Oxidant and Aerosol Study (SOAS) at the Look Rock, Tennessee  
549 ground site, *Atmos. Chem. Phys.*, 15, 8871-8888, doi:10.5194/acp-15-8871-2015, 2015.
- 550 Buxton, G. V., Malone, T. N., and Salmon, G. A.: Oxidation of glyoxal initiated by •OH in  
551 oxygenated aqueous solution, *J Chem. Soc. Faraday T.*, 93, 2889-2891, doi  
552 10.1039/A701468f, 1997.

553



554 Canagaratna, M. R., Jayne, J. T., Jimenez, J. L., Allan, J. D., Alfarra, M. R., Zhang, Q., Onasch,  
 555 T. B., Drewnick, F., Coe, H., Middlebrook, A., Delia, A., Williams, L. R., Trimborn, A.  
 556 M., Northway, M. J., DeCarlo, P. F., Kolb, C. E., Davidovits, P., Worsnop, D. R.:  
 557 Chemical and microphysical characterization of ambient aerosols with the Aerodyne  
 558 Aerosol Mass Spectrometer. *Mass Spectrometry Reviews*, 26, 185-222, doi:  
 559 10.1002/mas.20115, 2007.

560 Carlton, A. G., Turpin, B. J., Altieri, K. E., Seitzinger, S. P., Mathur, R., Roselle, S. J., and  
 561 Weber, R. J.: CMAQ model performance enhanced when in-cloud secondary organic  
 562 aerosol is included: Comparisons of organic carbon predictions with measurements,  
 563 *Environ. Sci. Technol.*, 42, 8789–8802, doi:10.1021/es801192n, 2008.

564 Carlton, A. G., Wiedinmyer, C., and Kroll, J. H.: A review of secondary organic aerosol (SOA)  
 565 formation from isoprene, *Atmos. Chem. Phys.*, 9, 4987-5005, doi:10.5194/acp-9-4987-  
 566 2009, 2009.

567 Carlton, A. G., and Turpin, B. J.: Particle partitioning potential of organic compounds is highest  
 568 in the Eastern US and driven by anthropogenic water, *Atmos. Chem. Phys.*, 13, 10203-  
 569 10214, doi:10.5194/acp-13-10203-2013, 2013.

570 Cazorla, M., Wolfe, G. M., Bailey, S. A., Swanson, A. K., Arkinson, H. L., and Hanisco, T. F.: A  
 571 new airborne laser-induced fluorescence instrument for in situ detection of formaldehyde  
 572 throughout the troposphere and lower stratosphere, *Atmos. Meas. Tech.*, 8, 541-552,  
 573 doi:10.5194/amt-8-541-2015, 2015.

574 Chan, A. W. H., Chan, M. N., Surratt, J. D., Chhabra, P. S., Loza, C. L., Crounse, J. D., Yee, L.  
 575 D., Flagan, R. C., Wennberg, P. O., and Seinfeld, J. H.: Role of aldehyde chemistry and  
 576 NO<sub>x</sub> concentrations in secondary organic aerosol formation, *Atmos. Chem. Phys.*, 10,  
 577 7169-7188, doi:10.5194/acp-10-7169-2010, 2010.

578 Cole-Filipiak, N. C., O'Connor, A. E., and Elrod, M. J.: Kinetics of the hydrolysis of  
 579 atmospherically relevant isoprene-derived hydroxy epoxides, *Environ. Sci. Technol.*, 44,  
 580 6718-6723, doi:10.1021/es1019228, 2010.

581 Darer, A. I., Cole-Filipiak, N. C., O'Connor, A. E., and Elrod, M. J.: Formation and stability of  
 582 atmospherically relevant isoprene-derived organosulfates and organonitrates, *Environ. Sci.*  
 583 *Technol.*, 45, 1895-1902, doi:10.1021/es103797z, 2011.

584 DeCarlo, P. F., Kimmel, J. R., Trimborn, A., Northway, M. J., Jayne, J. T., Aiken, A. C., Gonin,  
 585 M., Fuhrer, K., Horvath, T., Docherty, K. S., Worsnop, D. R., and Jimenez, J. L.: Field-  
 586 deployable, High-Resolution, Time-of-Flight Aerosol Mass Spectrometer, *Anal. Chem.*, 78,  
 587 8281-8289, doi: 10.1021/ac061249n, 2006.

588 Dommen, J., Metzger, A., Duplissy, J., Kalberer, M., Alfarra, M. R., Gascho, A., Weingartner,  
 589 E., Prévôt, A. S. H., Verheggen, B., and Baltensperger, U.: Laboratory observation of  
 590 oligomers in the aerosol from isoprene/NO<sub>x</sub> photooxidation, *Geophys. Res. Lett.*, 33,  
 591 L13805, doi:10.1029/2006gl026523, 2006.

592 Donahue, N. M., Robinson, A. L., Stanier, C. O., and Pandis, S. N.: Coupled partitioning,  
 593 dilution, and chemical aging of semivolatile organics, *Environ. Sci. Technol.*, 40, 2635-  
 594 2643, doi:10.1021/es052297c, 2006.

595 Drury, E., Jacob, D. J., Spurr, R. J. D., Wang, J., Shinozuka, Y., Anderson, B. E., Clarke, A. D.,  
 596 Dibb, J., McNaughton, C., and Weber, R.: Synthesis of satellite (MODIS), aircraft  
 597 (ICARTT), and surface (IMPROVE, EPA-AQS, AERONET) aerosol observations over  
 598 eastern North America to improve MODIS aerosol retrievals and constrain surface aerosol  
 599 concentrations and sources, *J. Geophys. Res.*, 115, D14204, doi:10.1029/2009jd012629,  
 600 2010.

601 EPA: U. S. Environmental Protection Agency, Technical Support Document (TSD): Preparation  
 602 of Emissions Inventories for the Version 6.1, 2011 Emissions Modeling Platform, available  
 603 at: [http://www.epa.gov/ttn/chief/emch/2011v6/2011v6.1\\_2018\\_2025\\_base\\_EmisMod\\_TSD](http://www.epa.gov/ttn/chief/emch/2011v6/2011v6.1_2018_2025_base_EmisMod_TSD_nov2014_v6.pdf)  
 604 [\\_nov2014\\_v6.pdf](http://www.epa.gov/ttn/chief/emch/2011v6/2011v6.1_2018_2025_base_EmisMod_TSD_nov2014_v6.pdf) (Accessed on July 15, 2015), 2014.

605 Eddingsaas, N. C., VanderVelde, D. G., and Wennberg, P. O.: Kinetics and products of the acid-  
 606 catalyzed ring-opening of atmospherically relevant butyl epoxy alcohols, *J. Phys. Chem. A*,  
 607 114, 8106-8113, doi:10.1021/jp103907c, 2010.

608 Edney, E. O., Kleindienst, T. E., Jaoui, M., Lewandowski, M., Offenberg, J. H., Wang, W., and  
 609 Claeys, M.: Formation of 2-methyl tetrols and 2-methylglyceric acid in secondary organic  
 610 aerosol from laboratory irradiated isoprene/NO<sub>x</sub>/SO<sub>2</sub>/air mixtures and their detection in  
 611 ambient PM<sub>2.5</sub> samples collected in the eastern United States, *Atmos. Environ.*, 39, 5281-  
 612 5289, doi:10.1016/j.atmosenv.2005.05.031, 2005.

613 Ervens, B., Gligorovski, S., and Herrmann, H.: Temperature-dependent rate constants for  
 614 hydroxyl radical reactions with organic compounds in aqueous solutions, *Phys. Chem.*  
 615 *Chem. Phys.*, 5, 1811-1824, doi:10.1039/b300072a, 2003.

616 Ervens, B., Turpin, B. J., and Weber, R. J.: Secondary organic aerosol formation in cloud  
 617 droplets and aqueous particles (aqSOA): A review of laboratory, field and model studies,  
 618 *Atmos. Chem. Phys.*, 11, 11069-11102, doi:10.5194/acp-11-11069-2011, 2011.

619 Fisher, J. A., Jacob, D., Travis, K. R., Kim, P. S., Marais, E. A., Miller, C. C., Yu, K., Zhu, L.,  
 620 Yantosca, R. M., Sulprizio, M. P., Mao, J., Wennberg, P. O., Crounse, J. D., Teng, A. P.,  
 621 Nguyen, T. B., Cohen, R. C., Romer, P., Nault, B. A., Jimenez, J. L., Campuzano-Jost, P.,  
 622 Shepson, P. B., Xiong, F., Blake, D. R., Goldstein, A. H., Hanisco, T. F., Ryerson, T. B.,  
 623 Wisthaler, A., and Mikoviny, T.: Organic nitrate chemistry and its implications for nitrogen  
 624 budgets in and isoprene- and monoterpene-rich atmosphere: constraints from aircraft  
 625 (SEAC<sup>4</sup>RS) and ground-based (SOAS) observations in the Southeast US, in preparation,  
 626 2016.

627 Fountoukis, C., and Nenes, A.: ISORROPIA II: A computationally efficient thermodynamic  
 628 equilibrium model for K<sup>+</sup>-Ca<sup>2+</sup>-Mg<sup>2+</sup>-NH<sub>4</sub><sup>+</sup>-Na<sup>+</sup>-SO<sub>4</sub><sup>2-</sup>-NO<sub>3</sub><sup>-</sup>-Cl<sup>-</sup>-H<sub>2</sub>O aerosols, *Atmos.*  
 629 *Chem. Phys.*, 7, 4639-4659, doi:10.5194/acp-7-4639-2007, 2007.

630 Fu, T.-M., Jacob, D. J., Wittrock, F., Burrows, J. P., Vrekoussis, M., and Henze, D. K.: Global  
 631 budgets of atmospheric glyoxal and methylglyoxal, and implications for formation of  
 632 secondary organic aerosols, *J. Geophys. Res.*, 113, D15303, doi:10.1029/2007jd009505,  
 633 2008.

634 Fu, T.-M., Jacob, D. J., and Heald, C. L.: Aqueous-phase reactive uptake of dicarbonyls as a  
 635 source of organic aerosol over eastern North America, *Atmos. Environ.*, 43, 1814-1822,  
 636 doi:10.1016/j.atmosenv.2008.12.029, 2009.

637 Gaston, C. J., Riedel, T. P., Zhang, Z., Gold, A., Surratt, J. D., and Thornton, J. A.: Reactive  
638 uptake of an isoprene-derived epoxydiol to submicron aerosol particles, *Environ. Sci.*  
639 *Technol.*, 48, 11178-11186, doi:10.1021/es5034266, 2014.

640 González Abad, G. G., Liu, X., Chance, K., Wang, H., Kurosu, T. P., and Suleiman, R.: Updated  
641 Smithsonian Astrophysical Observatory Ozone Monitoring Instrument (SAO OMI)  
642 formaldehyde retrieval, *Atmos. Meas. Tech.*, 8, 19-32, doi:10.5194/amt-8-19-2015, 2015.

643 Guenther, A., Karl, T., Harley, P., Wiedinmyer, C., Palmer, P. I., and Geron, C.: Estimates of  
644 global terrestrial isoprene emissions using MEGAN (Model of Emissions of Gases and  
645 Aerosols from Nature), *Atmos. Chem. Phys.*, 6, 3181-3210, doi:10.5194/acp-6-3181-2006,  
646 2006.

647 Guenther, A. B., Jiang, X., Heald, C. L., Sakulyanontvittaya, T., Duhl, T., Emmons, L. K., and  
648 Wang, X.: The Model of Emissions of Gases and Aerosols from Nature version 2.1  
649 (MEGAN2.1): An extended and updated framework for modeling biogenic emissions,  
650 *Geosci. Model Dev.*, 5, 1471-1492, doi:10.5194/gmd-5-1471-2012, 2012.

651 Guo, H., Xu, L., Bougiatioti, A., Cerully, K. M., Capps, S. L., Hite Jr., J. R., Carlton, A. G., Lee,  
652 S.-H., Bergin, M. H., Ng, N. L., Nenes, A., and Weber, R. J.: Fine-particle water and pH in  
653 the southeastern United States, *Atmos. Chem. Phys.*, 15, 5211-5228, doi:10.5194/acp-15-  
654 5211-2015, 2015.

655 Hallquist, M., Wenger, J. C., Baltensperger, U., Rudich, Y., Simpson, D., Claeys, M., Dommen,  
656 J., Donahue, N. M., George, C., Goldstein, A. H., Hamilton, J. F., Herrmann, H.,  
657 Hoffmann, T., Iinuma, Y., Jang, M., Jenkin, M. E., Jimenez, J. L., Kiendler-Scharr, A.,  
658 Maenhaut, W., McFiggans, G., Mentel, Th. F., Monod, A., Prévôt, A. S. H., Seinfeld, J. H.,  
659 Surratt, J. D., Szmigielski, R., and Wildt, J.: The formation, properties and impact of  
660 secondary organic aerosol: Current and emerging issues, *Atmos. Chem. Phys.*, 9, 5155-  
661 5236, doi:10.5194/acp-9-5155-2009, 2009.

662 Hess, M., Koepke, P., and Schult, I.: Optical properties of aerosols and clouds: The software  
663 package OPAC, *B. Am. Meteorol. Soc.*, 79, 831-844, 1998.

664 Hodzic, A., and Jimenez, J. L.: Modeling anthropogenically controlled secondary organic  
665 aerosols in a megacity: A simplified framework for global and climate models, *Geosci.*  
666 *Model. Dev.*, 4, 901-917, doi:10.5194/gmd-4-901-2011, 2011.

667 Hu, K. S., Darer, A. I., and Elrod, M. J.: Thermodynamics and kinetics of the hydrolysis of  
668 atmospherically relevant organonitrates and organosulfates, *Atmos. Chem. Phys.*, 11, 8307-  
669 8320, doi:10.5194/acp-11-8307-2011, 2011.

670 Hu, W. W., Campuzano-Jost, P., Palm, B. B., Day, D. A., Ortega, A. M., Hayes, P. L.,  
671 Krechmer, J. E., Chen, Q., Kuwata, M., Liu, Y. J., de Sá, S. S., Martin, S. T., Hu, M.,  
672 Budisulistiorini, S. H., Riva, M., Surratt, J. D., St. Clair, J. M., Isaacman-Van Wertz, G.,  
673 Yee, L. D., Goldstein, A. H., Carbone, S., Artaxo, P., de Gouw, J. A., Koss, A., Wisthaler,  
674 A., Mikoviny, T., Karl, T., Kaser, L., Jud, W., Hansel, A., Docherty, K. S., Robinson, N. H.,  
675 Coe, H., Allan, J. D., Canagaratna, M. R., Paulot, F., and Jimenez, J. L.: Characterization  
676 of a real-time tracer for isoprene epoxydiols-derived secondary organic aerosol (IEPOX-  
677 SOA) from aerosol mass spectrometer measurements, *Atmos. Chem. Phys.*, 15, 11807-  
678 11833, doi:10.5194/acp-15-11807-2015, 2015.

679 Jacob, D. J.: Heterogeneous chemistry and tropospheric ozone, *Atmos. Environ.*, 34, 2131-2159,  
680 doi:10.1016/s1352-2310(99)00462-8, 2000.

681 Jacobs, M. I., Darer, A. I., and Elrod, M. J.: Rate constants and products of the OH reaction with  
682 isoprene-derived epoxides, *Environ. Sci. Technol.*, 47, 12868-12876,  
683 doi:10.1021/es403340g, 2013.

684 Jacobs, M. I., Burke, W. J., and Elrod, M. J.: Kinetics of the reactions of isoprene-derived  
685 hydroxynitrates: Gas phase epoxide formation and solution phase hydrolysis, *Atmos.*  
686 *Chem. Phys.*, 14, 8933-8946, doi:10.5194/acp-14-8933-2014, 2014.

687 Kim, P. S., Jacob, D. J., Fisher, J. A., Travis, K., Yu, K., Zhu, L., Yantosca, R. M., Sulprizio, M.  
688 P., Jimenez, J. L., Campuzano-Jost, P., Froyd, K. D., Liao, J., Hair, J. W., Fenn, M. A.,  
689 Butler, C. F., Wagner, N. L., Gordon, T. D., Welti, A., Wennberg, P. O., Crounse, J. D., St.  
690 Clair, J. M., Teng, A. P., Millet, D. B., Schwarz, J. P., Markovic M. Z., and Perring, A. E.:  
691 Sources, seasonality, and trends of southeast US aerosol: an integrated analysis of surface,  
692 aircraft, and satellite observations with the GEOS-Chem chemical transport model, *Atmos.*  
693 *Chem. Phys.*, 15, 10411-10433, doi:10.5194/acpd-15-10411-2015, 2015.

694 King, S. M., Rosenoern, T., Shilling, J. E., Chen, Q., Wang, Z., Biskos, G., McKinney, K. A.,  
695 Pöschl, U., and Martin, S. T.: Cloud droplet activation of mixed organic-sulfate particles  
696 produced by the photooxidation of isoprene, *Atmos. Chem. Phys.*, 10, 3953-3964,  
697 doi:10.5194/acp-10-3953-2010, 2010.

698 Kleindienst, T. E., Edney, E. O., Lewandowski, M., Offenberg, J. H., and Jaoui, M.: Secondary  
699 organic carbon and aerosol yields from the irradiations of isoprene and  $\alpha$ -pinene in the  
700 presence of NO<sub>x</sub> and SO<sub>2</sub>, *Environ. Sci. Technol.*, 40, 3807-3812, doi:10.1021/es052446r,  
701 2006.

702 Kleindienst, T. E., Lewandowski, M., Offenberg, J. H., Jaoui, M., and Edney, E. O.: Ozone-  
703 isoprene reaction: Re-examination of the formation of secondary organic aerosol, *Geophys.*  
704 *Res. Lett.*, 34, L01805, doi:10.1029/2006gl027485, 2007.

705 Kleindienst, T. E., Lewandowski, M., Offenberg, J. H., Jaoui, M., and Edney, E. O.: The  
706 formation of secondary organic aerosol from the isoprene + OH reaction in the absence of  
707 NO<sub>x</sub>, *Atmos. Chem. Phys.*, 9, 6541-6558, doi:10.5194/acp-9-6541-2009, 2009.

708 Knote, C., Hodzic, A., Jimenez, J. L., Volkamer, R., Orlando, J. J., Baidar, S., Brioude, J., Fast,  
709 J., Gentner, D. R., Goldstein, A. H., Hayes, P. L., Knighton, W. B., Oetjen, H., Setyan, A.,  
710 Stark, H., Thalman, R., Tyndall, G., Washenfelder, R., Waxman, E., and Zhang, Q.:  
711 Simulation of semi-explicit mechanisms of SOA formation from glyoxal in aerosol in a 3-  
712 D model, *Atmos. Chem. Phys.*, 14, 6213-6239, doi:10.5194/acp-14-6213-2014, 2014.

713 Koepke, P., Hess, M., Schult, I., and Shettle, E. P.: Global aerosol data set, report, Max-Planck  
714 Inst. für Meteorol., Hamburg, Germany, 1997.

715 Krechmer, J. E., Coggon, M. M., Massoli, P., Nguyen, T. B., Crounse, J. D., Hu, W., Day, D. A.,  
716 Tyndall, G. S., Henze, D. K., Rivera-Rios, J. C., Nowak, J. B., Kimmel, J. R., Mauldin, III,  
717 R. L., Stark, H., Jayne, J. T., Sipilä, M., Junninen, H., St. Clair, J. M., Zhang, X., Feiner, P.  
718 A., Zhang, L., Miller, D. O., Brune, W. H., Keutsch, F. N., Wennberg, P. O., Seinfeld, J.  
719 H., Worsnop, D. R., Jimenez, J. L., and Canagaratna, M. R.: Formation of low volatility  
720 organic compounds and secondary organic aerosol from isoprene hydroxyhydroperoxide

low-NO oxidation, *Environ. Sci. Technol.*, 49, 10330-10339, doi:10.1021/acs.est.5b02031, 2015.

Kroll, J. H., Ng, N. L., Murphy, S. M., Flagan, R. C., and Seinfeld, J. H.: Secondary organic aerosol formation from isoprene photooxidation under high-NO<sub>x</sub> conditions, *Geophys. Res. Lett.*, 32, L18808, doi:10.1029/2005gl023637, 2005.

Kroll, J. H., Ng, N. L., Murphy, S. M., Flagan, R. C., and Seinfeld, J. H.: Secondary organic aerosol formation from isoprene photooxidation, *Environ. Sci. Technol.*, 40, 1869-1877, doi:10.1021/es0524301, 2006.

Lee, L., Teng, A. P., Wennberg, P. O., Crounse, J. D., and Cohen, R. C.: On rates and mechanisms of OH and O<sub>3</sub> reactions with isoprene-derived hydroxy nitrates, *J. Phys. Chem. A*, 118, 1622-1637, doi:10.1021/jp4107603, 2014.

Lewandowski, M., Jaoui, M., Offenberg, J. H., Krug, J. D., and Kleindienst, T. E.: Atmospheric oxidation of isoprene and 1,3-butadiene: Influence of aerosol acidity and relative humidity on secondary organic aerosol, *Atmos. Chem. Phys.*, 15, 3773-3783, doi:10.5194/acp-15-3773-2015, 2015.

Liao, J., Froyd, K. D., Murphy, D. M., Keutsch, F. N., Yu, G., Wennberg, P. O., St Clair, J. M., Crounse, J. D., Wisthaler, A., Mikoviny, T., Jimenez, J. L., Campuzano-Jost, P., Day, D. A., Hu, W., Ryerson, T. B., Pollack, I. B., Peischl, J., Anderson, B. E., Ziemba, L. D., Blake, D. R., Meinardi, S., and Diskin, G.: Airborne measurements of organosulfates over the continental U.S., *J. Geophys. Res.*, 120, 2990-3005, doi:10.1002/2014jd022378, 2015.

Liggio, J., Li, S.-M., and McLaren, R.: Reactive uptake of glyoxal by particulate matter, *J. Geophys. Res.*, 110, D10304, doi:10.1029/2004jd005113, 2005.

Lin, Y.-H., Zhang, H., Pye, H. O. T., Zhang, Z. F., Marth, W. J., Park, S., Arashiro, M., Cui, T., Budisulistiorini, S. H., Sexton, K. G., Vizuete, W., Xie, Y., Luecken, D. J., Piletic, I. R., Edney, E. O., Bartolotti, L. J., Gold, A., and Surratt, J. D.: Epoxide as a precursor to secondary organic aerosol formation from isoprene photooxidation in the presence of nitrogen oxides, *P. Natl. Acad. Sci. USA*, 110, 6718-6723, doi:10.1073/pnas.1221150110, 2013.

Liu, Y. J., Herdinger-Blatt, I., McKinney, K. A., and Martin, S. T.: Production of methyl vinyl ketone and methacrolein via the hydroperoxyl pathway of isoprene oxidation, *Atmos. Chem. Phys.*, 13, 5715-5730, doi:10.5194/acp-13-5715-2013, 2013.

Lin, G., S. Sillman, J. E. Penner, and A. Ito, Global modeling of SOA: the use of different mechanisms for aqueous-phase formation, *Atmos. Chem. Phys.*, 14, 5451-5475, doi:10.5194/acp-14-5451-2014, 2014.

Liu, J., L. W. Horowitz, S. Fan, A. G. Carlton, and H. Levy II, Global in-cloud production of secondary organic aerosols: implementation of a detailed chemical mechanism in the GFDL atmospheric model AM3, *J. Geophys. Res.*, D117, D15303, doi:10.1029/2012JD017838, 2012.

Mao, J., Paulot, F., Jacob, D. J., Cohen, R. C., Crounse, J. D., Wennberg, P. O., Keller, C. A., Hudman, R. C., Barkley, M. P., and Horowitz, L. W.: Ozone and organic nitrates over the eastern United States: Sensitivity to isoprene chemistry, *J. Geophys. Res.*, 118, 11256-11268, doi:10.1002/jgrd.50817, 2013.

763 Martin, R. V., Jacob, D. J., Yantosca, R. M., Chin, M., and Ginoux, P.: Global and regional  
 764 decreases in tropospheric oxidants from photochemical effects of aerosols, *J. Geophys.*  
 765 *Res.*, 108, 4097, doi:10.1029/2002jd002622, 2003.

766 McNeill, V. F., Woo, J. L., Kim, D. D., Schwier, A. N., Wannell, N. J., Sumner, A. J., and  
 767 Barakat, J. M.: Aqueous-phase secondary organic aerosol and organosulfate formation in  
 768 atmospheric aerosols: A modeling study, *Environ. Sci. Technol.*, 46, 8075-8081,  
 769 doi:10.1021/es3002986, 2012.

770 McNeill, V. F., Sareen, N., and Schwier, A. N.: Surface-active organics in atmospheric aerosols,  
 771 *Top. Curr. Chem.*, 339, 201-259, doi:10.1007/128\_2012\_404, 2014.

772 Millet, D. B., Jacob, D. J., Turquety, S., Hudman, R. C., Wu, S., Fried, A., Walega, J., Heikes, B.  
 773 G., Blake, D. R., Singh, H. B., Anderson, B. E., and Clarke, A. D.: Formaldehyde  
 774 distribution over North America: Implications for satellite retrievals of formaldehyde  
 775 columns and isoprene emission, *J. Geophys. Res.*, 111, D24S02,  
 776 doi:10.1029/2005jd006853, 2006.

777 Myriokefalitakis, S., Tsigaridas, K., Mihalopoulos, N., Sciare, J., Nenes, A., Kawamura, K.,  
 778 Segers, A., and Kanakidou, M.: In-cloud oxalate formation in the global troposphere: a 3-D  
 779 modeling study, *Atmos. Chem. Phys.*, 11, 5761-5782, doi:10.5194/acp-11-5761-2011,  
 780 2011.

781 Ng, N. L., Kwan, A. J., Surratt, J. D., Chan, A. W. H., Chhabra, P. S., Sorooshian, A., Pye, H. O.  
 782 T., Crounse, J. D., Wennberg, P. O., Flagan, R. C., and Seinfeld, J. H.: Secondary organic  
 783 aerosol (SOA) formation from reaction of isoprene with nitrate radicals ( $\text{NO}_3$ ), *Atmos.*  
 784 *Chem. Phys.*, 8, 4117-4140, doi:10.5194/acp-8-4117-2008, 2008.

785 Nguyen, T. B., Coggon, M. M., Bates, K. H., Zhang, X., Schwantes, R. H., Schilling, K. A.,  
 786 Loza, C. L., Flagan, R. C., Wennberg, P. O., and Seinfeld, J. H.: Organic aerosol formation  
 787 from the reactive uptake of isoprene epoxydiols (IEPOX) onto non-acidified inorganic  
 788 seeds, *Atmos. Chem. Phys.*, 14, 3497-3510, doi:10.5194/acp-14-3497-2014, 2014.

789 Nguyen, T. B., Crounse, J. D., Teng, A. P., St. Clair, J. M., Paulot, F., Wolfe, G. M., and  
 790 Wennberg, P. O.: Rapid deposition of oxidized biogenic compounds to a temperate forest,  
 791 *P. Natl. Acad. Sci. USA*, 112, E392-E401, doi:10.1073/pnas.1418702112, 2015a.

792 Nguyen, T. B., Bates, K. H., Crounse, J. D., Schwantes, R. H., Zhang, X., Kjaergaard, H. G.,  
 793 Surratt, J. D., Lin, P., Laskin, A., Seinfeld, J. H., and Wennberg, P. O.: Mechanism of the  
 794 hydroxyl radical oxidation of methacryloyl peroxyxynitrate (MPAN) and its pathway toward  
 795 secondary organic aerosol formation in the atmosphere, *Phys Chem Chem Phys*, 17, 17914-  
 796 17926, doi:10.1039/c5cp02001h, 2015b.

797 Nozière, B., Dziedzic, P., and Córdoba, A.: Products and kinetics of the liquid-phase reaction of  
 798 glyoxal catalyzed by ammonium ions ( $\text{NH}_4^+$ ), *J. Phys. Chem. A*, 113, 231-237,  
 799 doi:10.1021/jp8078293, 2009.

800 Odum, J. R., Hoffmann, T., Bowman, F., Collins, D., Flagan, R. C., and Seinfeld, J. H.:  
 801 Gas/particle partitioning and secondary organic aerosol yields, *Environ. Sci. Technol.*, 30,  
 802 2580-2585, doi:10.1021/es950943+, 1996.

803 Palmer, P. I., Jacob, D. J., Fiore, A. M., Martin, R. V., Chance, K., and Kurosu, T. P.: Mapping  
 804 isoprene emissions over North America using formaldehyde column observations from  
 805 space, *J. Geophys. Res.*, 108, 4180, doi:10.1029/2002jd002153, 2003.

806 Palmer, P. I., Abbot, D. S., Fu, T.-M., Jacob, D. J., Chance, K., Kurosu, T. P., Guenther, A.,  
 807 Wiedinmyer, C., Stanton, J. C., Pilling, M. J., Pressley, S. N., Lamb, B., and Sumner, A. L.:  
 808 Quantifying the seasonal and interannual variability of North American isoprene emissions  
 809 using satellite observations of the formaldehyde column, *J. Geophys. Res.*, 111, D12315,  
 810 doi:10.1029/2005jd006689, 2006.

811 Paulot, F., Crounse, J. D., Kjaergaard, H. G., Kroll, J. H., Seinfeld, J. H., and Wennberg, P. O.:  
 812 Isoprene photooxidation: New insights into the production of acids and organic nitrates,  
 813 *Atmos. Chem. Phys.*, 9, 1479-1501, doi:10.5194/acp-9-1479-2009, 2009a.

814 Paulot, F., Crounse, J. D., Kjaergaard, H. G., Kürten, A., St Clair, J. M., Seinfeld, J. H., and  
 815 Wennberg, P. O.: Unexpected epoxide formation in the gas-phase photooxidation of  
 816 isoprene, *Science*, 325, 730-733, doi:10.1126/science.1172910, 2009b.

817 Peeters, J., Nguyen, T. L., and Vereecken, L.: HO<sub>x</sub> radical regeneration in the oxidation of  
 818 isoprene, *Phys. Chem. Chem. Phys.*, 11, 5935-5939, doi:10.1039/b908511d, 2009.

819 Peeters, J., and Müller, J.-F.: HO<sub>x</sub> radical regeneration in isoprene oxidation via peroxy radical  
 820 isomerisations. II: Experimental evidence and global impact, *Phys. Chem. Chem. Phys.*, 12,  
 821 14227-14235, doi:10.1039/c0cp00811g, 2010.

822 Piletic, I. R., Edney, E. O., and Bartolotti, L. J.: A computational study of acid catalyzed aerosol  
 823 reactions of atmospherically relevant epoxides, *Phys. Chem. Chem. Phys.*, 15, 18065-  
 824 18076, doi:10.1039/c3cp52851k, 2013.

825 Pye, H. O. T., Chan, A. W. H., Barkley, M. P., and Seinfeld, J. H.: Global modeling of organic  
 826 aerosol: The importance of reactive nitrogen (NO<sub>x</sub> and NO<sub>3</sub>), *Atmos. Chem. Phys.*, 10,  
 827 11261-11276, doi:10.5194/acp-10-11261-2010, 2010.

828 Pye, H. O. T., Pinder, R. W., Piletic, I. R., Xie, Y., Capps, S. L., Lin, Y.-H., Surratt, J. D., Zhang,  
 829 Z., Gold, A., Luecken, D. J., Hutzell, W. T., Jaoui, M., Offenberg, J. H., Kleindienst, T. E.,  
 830 Lewandowski, M., and Edney, E. O.: Epoxide pathways improve model predictions of  
 831 isoprene markers and reveal key role of acidity in aerosol formation, *Environ. Sci.*  
 832 *Technol.*, 47, 11056-11064, doi:10.1021/es402106h, 2013.

833 Riedel, T. P., Lin, Y.-H., Budisulistiorini, S. H., Gaston, C. J., Thornton, J. A., Zhang, Z. F.,  
 834 Vizuete, W., Gold, A., and Surratt, J. D.: Heterogeneous reactions of isoprene-derived  
 835 epoxides: Reaction probabilities and molar secondary organic aerosol yield estimates,  
 836 *Environ. Sci. Technol. Lett.*, 2, 38-42, doi:10.1021/ez500406f, 2015.

837 Rollins, A. W., Kiendler-Scharr, A., Fry, J. L., Brauers, T., Brown, S. S., Dorn, H.-P., Dubé, W.  
 838 P., Fuchs, H., Mensah, A., Mentel, T. F., Rohrer, F., Tillmann, R., Wegener, R.,  
 839 Wooldridge, P. J., and Cohen, R. C.: Isoprene oxidation by nitrate radical: Alkyl nitrate and  
 840 secondary organic aerosol yields, *Atmos. Chem. Phys.*, 9, 6685-6703, doi:10.5194/acp-9-  
 841 6685-2009, 2009.

842 SEAC<sup>4</sup>RS Archive, doi:10.5067/Aircraft/SEAC4RS/Aerosol-TraceGas-Cloud.

843 Sato, K., Nakao, S., Clark, C. H., Qi, L., and Cocker III, D. R.: Secondary organic aerosol  
 844 formation from the photooxidation of isoprene, 1,3-butadiene, and 2,3-dimethyl-1,3-  
 845 butadiene under high NO<sub>x</sub> conditions, *Atmos. Chem. Phys.*, 11, 7301-7317,  
 846 doi:10.5194/acp-11-7301-2011, 2011.

847 Saxena, P., and Hildemann, L. M.: Water-soluble organics in atmospheric particles: A critical  
 848 review of the literature and application of thermodynamics to identify candidate  
 849 compounds, *J. Atmos. Chem.*, 24, 57-109, doi:10.1007/bf00053823, 1996.

850 Schwartz, S.E.: Mass-transport considerations pertinent to aqueous-phase reactions of gases in  
 851 liquid-water clouds. In: Jaechske, W. (Ed.), *Chemistry of Multiphase Atmospheric*  
 852 *Systems*, Springer, Heidelberg, pp. 415-471, 1986.

853 Scott, C. E., Rap, A., Spracklen, D. V., Forster, P. M., Carslaw, K. S., Mann, G. W., Pringle, K.  
 854 J., Kivekäs, N., Kulmala, M., Lihavainen, H., and Tunved, P.: The direct and indirect  
 855 radiative effects of biogenic secondary organic aerosol, *Atmos. Chem. Phys.*, 14, 447-470,  
 856 doi:10.5194/acp-14-447-2014, 2014.

857 Song, M., Liu, P. F., Hanna, S. J., Li, Y. J., Martin, S. T., and Bertram, A. K.: Relative humidity-  
 858 dependent viscosities of isoprene-derived secondary organic material and atmospheric  
 859 implications for isoprene-dominant forests, *Atmos. Chem. Phys.*, 15, 5145-5159,  
 860 doi:10.5194/acp-15-5145-2015, 2015.

861 Stavrou, T., Peeters, J., and Müller, J.-F.: Improved global modelling of HO<sub>x</sub> recycling in  
 862 isoprene oxidation: Evaluation against the GABRIEL and INTEx-A aircraft campaign  
 863 measurements, *Atmos. Chem. Phys.*, 10, 9863-9878, doi:10.5194/acp-10-9863-2010, 2010.

864 St. Clair, J. M., Rivera-Rios, J. C., Crounse, J. D., Knap, H. C., Bates, K. H., Teng, A. P.,  
 865 Jørgensen, S., Kjaergaard, H. G., Keutsch, F. N., Wennberg, P. O.: Kinetics and products  
 866 of the reaction of the first-generation isoprene hydroperoxide (ISOPPOOH) with OH, *J.*  
 867 *Phys. Chem. A*, doi:10.1021/acs.jpca.5b06532, 2016.

868 Sumner, A. J., Woo, J. L., and McNeill, V. F.: Model Analysis of secondary organic aerosol  
 869 formation by glyoxal in laboratory studies: The case for photoenhanced chemistry,  
 870 *Environ. Sci. Technol.*, 48, 11919-11925, doi:10.1021/es502020j, 2014.

871 Surratt, J. D., Murphy, S. M., Kroll, J. H., Ng, N. L., Hildebrandt, L., Sorooshian, A.,  
 872 Szmigielski, R., Vermeylen, R., Maenhaut, W., Claeys, M., Flagan, R. C., and Seinfeld, J.  
 873 H.: Chemical composition of secondary organic aerosol formed from the photooxidation of  
 874 isoprene, *J. Phys. Chem. A*, 110, 9665-9690, doi:10.1021/jp061734m, 2006.

875 Surratt, J. D., Lewandowski, M., Offenberg, J. H., Jaoui, M., Kleindienst, T. E., Edney, E. O.,  
 876 and Seinfeld, J. H.: Effect of acidity on secondary organic aerosol formation from isoprene,  
 877 *Environ. Sci. Technol.*, 41, 5363-5369, doi:10.1021/es0704176, 2007a.

878 Surratt, J. D., Kroll, J. H., Kleindienst, T. E., Edney, E. O., Claeys, M., Sorooshian, A., Ng, N.  
 879 L., Offenberg, J. H., Lewandowski, M., Jaoui, M., Flagan, R. C., and Seinfeld, J. H.:  
 880 Evidence for organosulfates in secondary organic aerosol, *Environ. Sci. Technol.*, 41, 517-  
 881 527, doi:10.1021/es062081q, 2007b.

882 Surratt, J. D., Chan, A. W. H., Eddingsaas, N. C., Chan, M., Loza, C. L., Kwan, A. J., Hersey, S.  
 883 P., Flagan, R. C., Wennberg, P. O., and Seinfeld, J. H.: Reactive intermediates revealed in



884 secondary organic aerosol formation from isoprene, *P. Natl. Acad. Sci. USA*, 107, 6640-  
885 6645, doi:10.1073/pnas.0911114107, 2010.

886 Tan, Y., Perri, M. J., Seitzinger, S. P., and Turpin, B. J.: Effects of precursor concentration and  
887 acidic sulfate in aqueous glyoxal-OH radical oxidation and implications for secondary  
888 organic aerosol, *Environ. Sci. Technol.*, 43, 8105-8112, doi:10.1021/es901742f, 2009.

889 Tan, Y., Carlton, A. G., Seitzinger, S. P., and Turpin, B. J.: SOA from methylglyoxal in clouds  
890 and wet aerosols: Measurement and prediction of key products, *Atmos. Environ.*, 44, 5218-  
891 5226, doi:10.1016/j.atmosenv.2010.08.045, 2010.

892 Toon, O. B. and the SEAC<sup>4</sup>RS science team: Planning, implementation, and scientific goals of  
893 the Studies of Emissions and Atmospheric Composition, Clouds, and Climate Coupling by  
894 Regional Surveys (SEAC<sup>4</sup>RS) field mission, submitted to *J. Geophys. Res.*, 2016.

895 Travis, K. R., Jacob, D. J., Fisher, J. A., Kim, P. S., Marais, E. A., Zhu, L., Miller, C. C.,  
896 Wennberg, P. O., Crounse, J., Hanisco, T. A., Ryerson, T., Yu, K., Wolfe, G. M.,  
897 Thompson, A., Mao, J., Paulot, F., Yantosca, R. M., Sulprizio, M., and Neuman, A.: NO<sub>x</sub>  
898 emissions, isoprene oxidation pathways, and implications for surface ozone in the  
899 Southeast United States, in preparation, 2016.

900 Virtanen, A., Joutsensaari, J., Koop, T., Kannosto, J., Yli-Pirilä, P., Leskinen, J., Mäkelä, J. M.,  
901 Holopainen, J. K., Pöschl, U., Kulmala, M., Worsnop, D. R., and Laaksonen, A.: An  
902 amorphous solid state of biogenic secondary organic aerosol particles, *Nature*, 467, 824-  
903 827, doi:10.1038/nature09455, 2010.

904 Volkamer, R., Martini, F. S., Molina, L. T., Salcedo, D., Jimenez, J. L., and Molina, M. J.: A  
905 missing sink for gas-phase glyoxal in Mexico City: Formation of secondary organic  
906 aerosol, *Geophys. Res. Lett.*, 34, L19807, doi:10.1029/2007gl030752, 2007.

907 Volkamer, R., Ziemann, P. J., and Molina, M. J.: Secondary organic aerosol formation from  
908 acetylene (C<sub>2</sub>H<sub>2</sub>): Seed effect on SOA yields due to organic photochemistry in the aerosol  
909 aqueous phase, *Atmos. Chem. Phys.*, 9, 1907-1928, doi:10.5194/acp-9-1907-2009, 2009.

910 Wagner, N. L., Brock, C. A., Angevine, W. M., Beyersdorf, A., Campuzano-Jost, P., Day, D., de  
911 Gouw, J. A., Diskin, G. S., Gordon, T. D., Graus, M. G., Holloway, J. S., Huey, G.,  
912 Jimenez, J. L., Lack, D. A., Liao, J., Liu, X., Markovic, M. Z., Middlebrook, A. M.,  
913 Mikoviny, T., Peischl, J., Perring, A. E., Richardson, M. S., Ryerson, T. B., Schwarz, J. P.,  
914 Warneke, C., Welti, A., Wisthaler, A., Ziemba, L. D., and Murphy, D. M.: In situ vertical  
915 profiles of aerosol extinction, mass, and composition over the southeast United States  
916 during SENEX and SEAC<sup>4</sup>RS: Observations of a modest aerosol enhancement aloft,  
917 *Atmos. Chem. Phys.*, 15, 7085-7102, doi:10.5194/acp-15-7085-2015, 2015.

918 Wang, J., Hoffmann, A. A., Park, R. J., Jacob, D. J., and Martin, S. T.: Global distribution of  
919 solid and aqueous sulfate aerosols: Effect of the hysteresis of particle phase transitions, *J.*  
920 *Geophys. Res.*, 113, D11206, doi:10.1029/2007jd009367, 2008.

921 Waxman, E. M., Dzepina, K., Ervens, B., Lee-Taylor, J., Aumont, B., Jimenez, J. L., Madronich,  
922 S., and Volkamer, R.: Secondary organic aerosol formation from semi- and intermediate-  
923 volatility organic compounds and glyoxal: Relevance of O/C as a tracer for aqueous  
924 multiphase chemistry, *Geophys. Res. Lett.*, 40, 978-982, doi:10.1002/grl.50203, 2013.

925 Xu, L., Kollman, M. S., Song, C., Shilling, J. E., and Ng, N. L.: Effects of NO<sub>x</sub> on the volatility  
 926 of secondary organic aerosol from isoprene photooxidation, *Environ. Sci. Technol.*, 48,  
 927 2253-2262, doi:10.1021/es404842g, 2014.

928 Xu, L., Guo, H., Boyd, C. M., Klein, M., Bougiatioti, A., Cerully, K. M., Hite, J. R., Isaacman-  
 929 VanWertz, G., Kreisberg, N. M., Knote, C., Olson, K., Koss, A., Goldstein, A. H., Hering,  
 930 S. V., de Gouw, J., Baumann, K., Lee, S.-H., Nenes, A., Weber, R. J., and Ng, N. L.:  
 931 Effects of anthropogenic emissions on aerosol formation from isoprene and monoterpenes  
 932 in the southeastern United States, *P. Natl. Acad. Sci. USA*, 112, 37-42,  
 933 doi:10.1073/pnas.1417609112, 2015.

934 Yu, K., Jacob, D. J., Fisher, J., Kim, P. S., Marais, E. A., Miller, C. C., Travis, K., Zhu, L.,  
 935 Yantosca, R. M., Sulprizio, M., Cohen, R. C., Dibb, J. E., Fried, A., Mikoviny, T., Ryerson,  
 936 T. B., Wennberg, P. O., and Wisthaler, A.: Sensitivity to grid resolution in the ability of a  
 937 chemical transport model to simulate observed oxidant chemistry under high-isoprene  
 938 conditions, submitted to *Atmos. Chem. Phys.*, 2016.

939 Zhang, Q., Jimenez, J. L., Canagaratna, M. R., Allan, J. D., Coe, H., Ulbrich, I., Alfarra, M. R.,  
 940 Takami, A., Middlebrook, A. M., Sun, Y. L., Dzepina, K., Dunlea, E., Docherty, K.,  
 941 DeCarlo, P. F., Salcedo, D., Onasch, T., Jayne, J. T., Miyoshi, T., Shimojo, A.,  
 942 Hatakeyama, S., Takegawa, N., Kondo, Y., Schneider, J., Drewnick, F., Borrmann, S.,  
 943 Weimer, S., Demerjian, K., Williams, P., Bower, K., Bahreini, R., Cottrell, L., Griffin, R.  
 944 J., Rautiainen, J., Sun, J. Y., Zhang, Y. M., and Worsnop, D. R.: Ubiquity and dominance  
 945 of oxygenated species in organic aerosols in anthropogenically-influenced Northern  
 946 Hemisphere midlatitudes, *Geophys. Res. Lett.*, 34, L13801, doi:10.1029/2007gl029979,  
 947 2007.

948 Zhang, H., Surratt, J. D., Lin, Y. H., Bapat, J., and Kamens, R. M.: Effect of relative humidity on  
 949 SOA formation from isoprene/NO photooxidation: Enhancement of 2-methylglyceric acid  
 950 and its corresponding oligoesters under dry conditions, *Atmos. Chem. Phys.*, 11, 6411-  
 951 6424, doi:10.5194/acp-11-6411-2011, 2011.

952 Zhang, H., Parikh, H. M., Bapat, J., Lin, Y. H., Surratt, J. D., and Kamens, R. M.: Modelling of  
 953 secondary organic aerosol formation from isoprene photooxidation chamber studies using  
 954 different approaches, *Environ. Chem.*, 10, 194-209, doi:10.1071/en13029, 2013.

955 Zhu, L., Jacob, D., Mickley, L., Kim, P. S., Fisher, J., Travis, K., Yu, K., Yantosca, R. M.,  
 956 Sulprizio, M., Fried, A., Hanisco, T., Wolfe, G., Abad, G. G., Chance, K., De Smedt, I.,  
 957 and Yang, K.: Indirect validation of new OMI, GOME-2, and OMPS formaldehyde  
 958 (HCHO) retrievals using SEAC<sup>4</sup>RS data, in preparation, 2016.

959 **TABLES**

960 **Table 1.** Constants for reactive uptake of isoprene SOA precursors <sup>a</sup>

Species <sup>b</sup>	$H^*$ [M atm <sup>-1</sup> ]	$k_{H+}$ [M <sup>-1</sup> s <sup>-1</sup> ]	$k_{nuc}$ [M <sup>-2</sup> s <sup>-1</sup> ]	$k_{HSO4-}$ [M <sup>-1</sup> s <sup>-1</sup> ]	$k_{aq}$ [s <sup>-1</sup> ]
IEPOX	$3.3 \times 10^7, ^c$	$3.6 \times 10^{-2}, ^d$	$2.0 \times 10^{-4}, ^e$	$7.3 \times 10^{-4}, ^e$	Equation (2)
ISOPN <sub>β</sub> <sup>f</sup>	$3.3 \times 10^5, ^g$	—	—	—	$1.6 \times 10^{-5}, ^h$
ISOPN <sub>δ</sub> <sup>f</sup>	$3.3 \times 10^5, ^g$	—	—	—	$6.8 \times 10^{-3}, ^h$
DHDN	$3.3 \times 10^5, ^g$	—	—	—	$6.8 \times 10^{-3}, ^i$

961 <sup>a</sup> Effective Henry's law constants  $H^*$  and aqueous-phase rate constants used to calculate reactive uptake  
 962 coefficients  $\gamma$  for isoprene SOA precursors IEPOX, ISOPN<sub>β</sub>, ISOPN<sub>δ</sub>, and DHDN following Eqs. (1) and  
 963 (2). Calculation of  $\gamma$  for other isoprene SOA precursors in Fig. 2 is described in the text.

964 <sup>b</sup> See Fig. 2 for definition of acronyms.

965 <sup>c</sup> Best fit to SOAS and SEAC<sup>4</sup>RS IEPOX SOA and consistent with Nguyen et al. (2014).

966 <sup>d</sup> Cole-Filipiak et al. (2010).

967 <sup>e</sup> Eddingsaas et al. (2010).

968 <sup>f</sup> ISOPN species formed from the beta and delta isoprene oxidation channels (Paulot et al., 2009a) are  
 969 treated separately in GEOS-Chem.

970 <sup>g</sup> By analogy with 4-nitrooxy-3-methyl-2-butanol (Rollins et al., 2009).

971 <sup>h</sup> Jacobs et al. (2014).

972 <sup>i</sup> Assumed same as for ISOPN<sub>δ</sub> (Hu et al., 2011).

973 **Table 2.** Mean reactive uptake coefficients  $\gamma$  of isoprene SOA precursors <sup>a</sup>

Species <sup>b</sup>	$\gamma$	pH dependence <sup>c</sup>			
		pH > 3	2 < pH < 3	1 < pH < 2	0 < pH < 1
IEPOX	$4.2 \times 10^{-3}$	$8.6 \times 10^{-7}$	$2.0 \times 10^{-4}$	$1.1 \times 10^{-3}$	$1.0 \times 10^{-2}$
MEPOX	$1.3 \times 10^{-4}$	$2.7 \times 10^{-8}$	$6.4 \times 10^{-6}$	$3.6 \times 10^{-5}$	$3.2 \times 10^{-4}$
ISOPN <sub>β</sub>	$1.3 \times 10^{-7}$	—			
ISOPN <sub>δ</sub>	$5.2 \times 10^{-5}$	—			
DHDN	$6.5 \times 10^{-5}$	—			
GLYX	$2.9 \times 10^{-3, d}$	—			
MGLY	$4.0 \times 10^{-7}$	—			
C <sub>5</sub> -LVOC	0.1	—			
NT-ISOPN	0.1	—			

974 <sup>a</sup> Mean values computed in GEOS-Chem for the Southeast US in summer as sampled along the boundary-  
975 layer (< 2 km) SEAC<sup>4</sup>RS aircraft tracks and applied to aqueous aerosol. The reactive uptake coefficient  $\gamma$   
976 is defined as the probability that a gas molecule colliding with an aqueous aerosol particle will be taken  
977 up and react in the aqueous phase to form non-volatile products.

978 <sup>b</sup> See Fig. 2 for definition of acronyms.

979 <sup>c</sup>  $\gamma$  for IEPOX and MEPOX are continuous functions of pH (Eq. (2)). Values shown here are averages for  
980 different pH ranges sampled along the SEAC<sup>4</sup>RS flight tracks. Aqueous aerosol pH is calculated locally  
981 in GEOS-Chem using the ISORROPIA thermodynamic model (Fountoukis and Nenes, 2007).

982 <sup>d</sup> Daytime value. Nighttime value is  $5 \times 10^{-6}$ .

## FIGURES

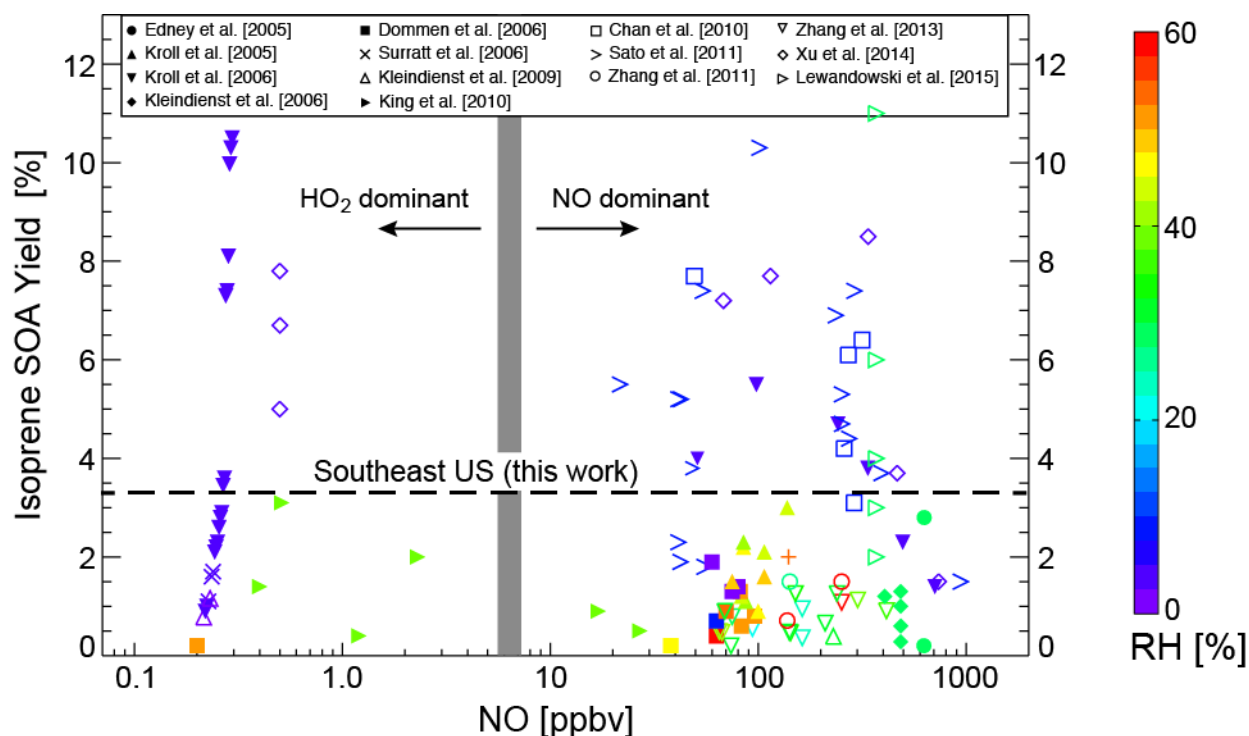


**Figure 1.** Yields of secondary organic aerosol (SOA) from isoprene oxidation as reported by chamber studies in the literature and plotted as a function of the initial NO concentration and relative humidity (RH). Yields are defined as the mass of SOA produced per unit mass of isoprene oxidized. For studies with no detectable NO we plot the NO concentration as half the reported instrument detection limit, and stagger points as needed for clarity. Data are colored by relative humidity (RH). The thick grey line divides the low-NO<sub>x</sub> and high-NO<sub>x</sub> pathways as determined by the fate of the ISOPO<sub>2</sub> radical (HO<sub>2</sub> dominant for the low-NO<sub>x</sub> pathway, NO dominant for the high-NO<sub>x</sub> pathway). The transition between the two pathways occurs at a higher NO concentration than in the atmosphere because HO<sub>2</sub> concentrations in the chambers are usually much higher. Also shown as dashed line is the mean atmospheric yield of 3.3% for the Southeast US determined in our study.



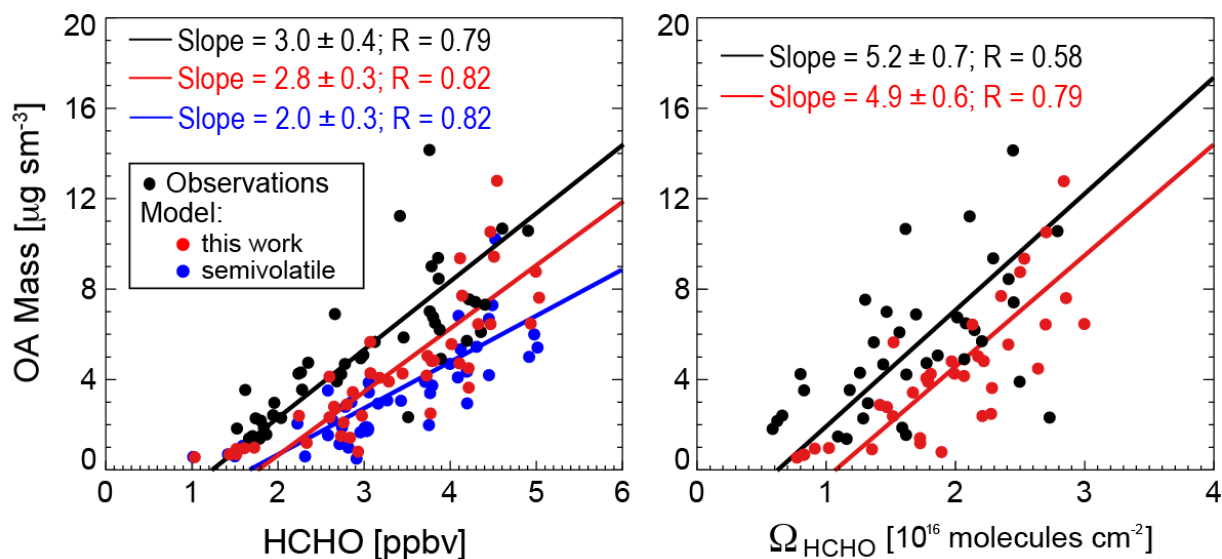


**Figure 3.** Relationship of organic aerosol (OA) and formaldehyde (HCHO) concentrations over the Southeast US in summer. The figure shows scatterplots of SEAC<sup>4</sup>RS aircraft observations of OA concentrations in the boundary layer (< 2 km) vs. HCHO mixing ratios measured from the aircraft (left), and column HCHO ( $\Omega_{\text{HCHO}}$ ) retrieved from OMI satellite observations (right). Individual points are data from individual SEAC<sup>4</sup>RS flight days (August 8 - September 10), averaged on the GEOS-Chem grid. OMI data are for SEAC<sup>4</sup>RS flight days and coincident with the flight tracks. GEOS-Chem is sampled for the corresponding locations and times. Results from our simulation with aqueous-phase isoprene SOA chemistry are shown in red, and results from a simulation with the Pye et al. (2010) semivolatile reversible partitioning scheme are shown in blue. Aerosol concentrations are per m<sup>3</sup> at standard conditions of temperature and pressure (STP: 273 K; 1 atm), denoted sm<sup>-3</sup>. Reduced major axis (RMA) regressions are also shown with regression parameters and Pearson's correlation coefficients given inset. 1 $\sigma$  standard deviations on the regression slopes are obtained with jackknife resampling.

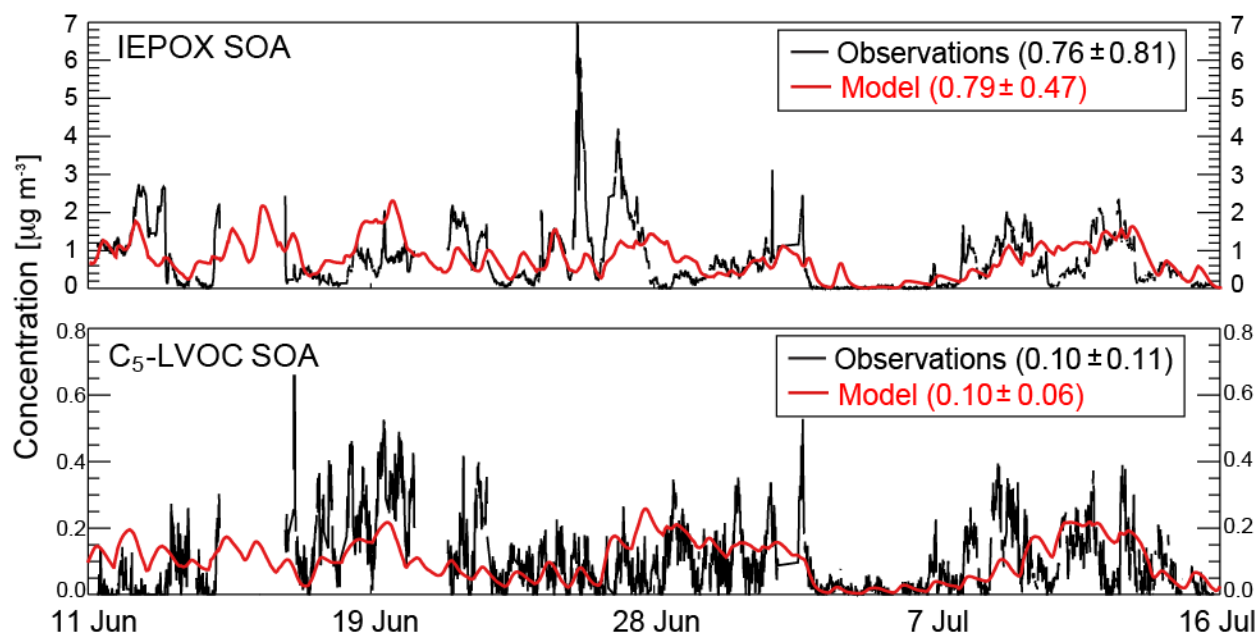
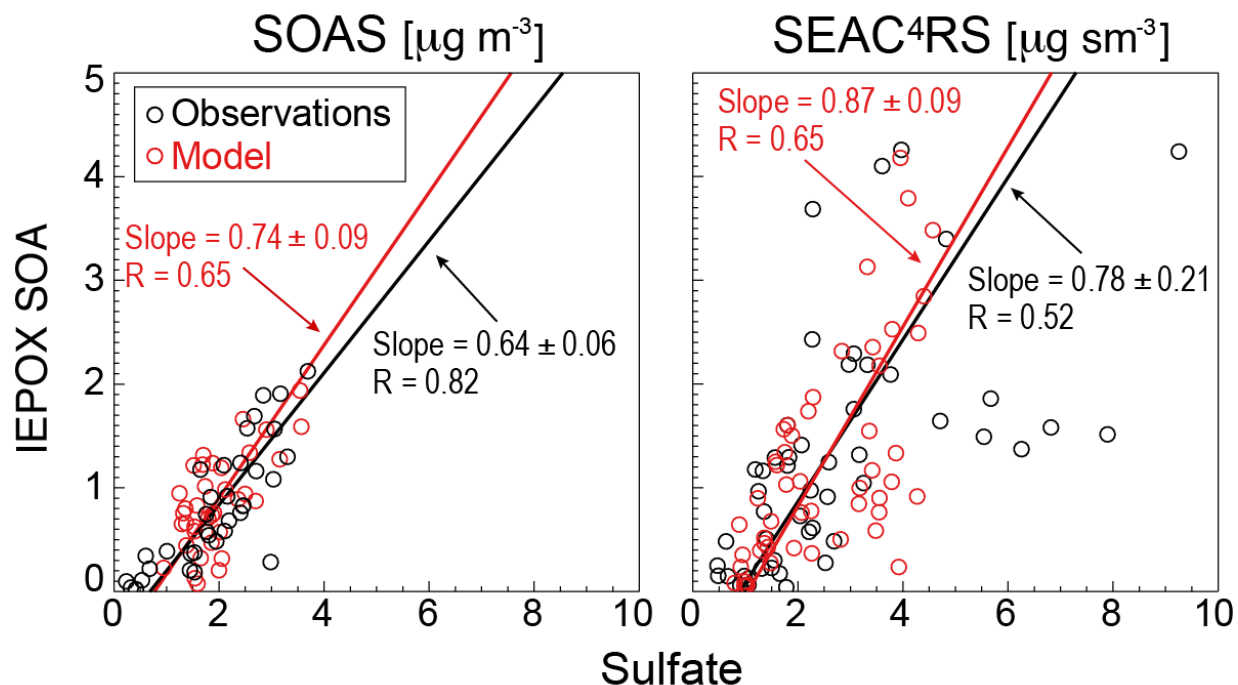


**Figure 4.** Time series of the concentrations of isoprene SOA components at the SOAS site in Centreville, Alabama (32.94°N; 87.18°W) in June-July 2013: measured (black) and modeled (red) IEPOX SOA (top) and C<sub>5</sub>-LVOC SOA (bottom) mass concentrations. Means and 1 $\sigma$  standard deviations are given for the observations and the model.





1028

1029 **Figure 5.** Relationship of IEPOX SOA and sulfate concentrations over the Southeast US in  
 1030 summer. Observed (black) and simulated (red) data are averages for each campaign day during  
 1031 SOAS (left), and boundary layer averages ( $< 2$  km) for  $2^\circ \times 2.5^\circ$  GEOS-Chem grid squares on  
 1032 individual flight days during SEAC<sup>4</sup>RS (right). RMA regression slopes and Pearson's correlation  
 1033 coefficients are shown.  $1\sigma$  standard deviations on the regression slopes are obtained with  
 1034 jackknife resampling.

## Boundary-layer IEPOX SOA and Sulfate Concentrations

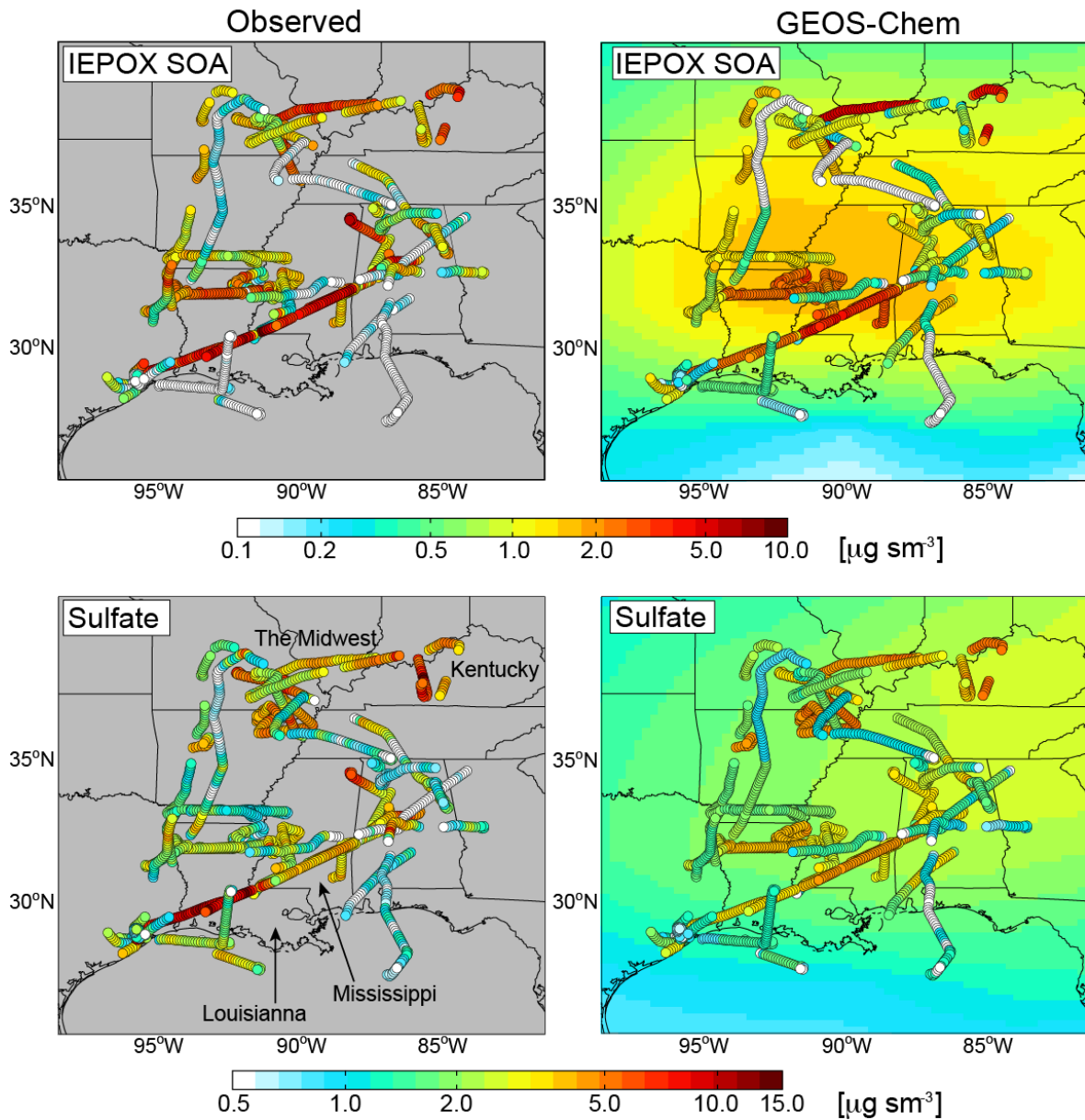


**Figure 6.** Spatial distributions of IEPOX SOA and sulfate concentrations in the boundary layer (<2 km) over the Southeast US during SEAC<sup>4</sup>RS (August-September 2013). Aircraft AMS observations of IEPOX SOA (top left) and sulfate (bottom left) are compared to model values sampled at the time and location of the aircraft observations (individual points) and averaged during the SEAC<sup>4</sup>RS period (background contours). Data are on a logarithmic scale.

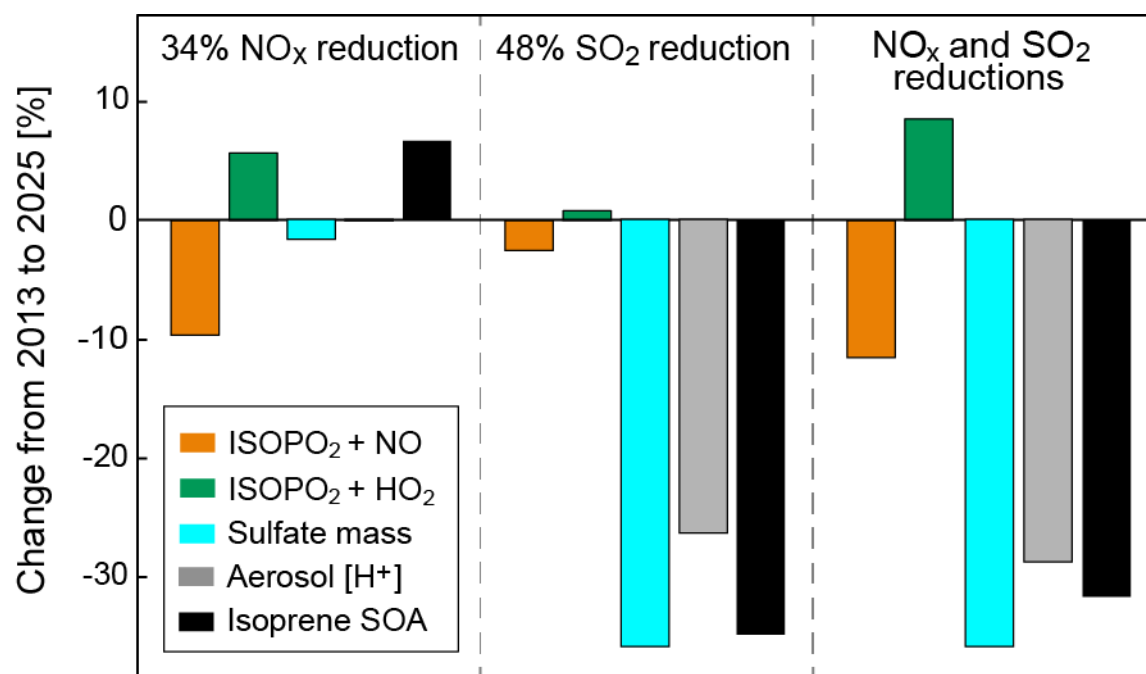


**Figure 7.** Effect of projected 2013-2025 reductions in US anthropogenic emissions on the formation of isoprene secondary organic aerosol (SOA). Emissions of NO<sub>x</sub> and SO<sub>2</sub> are projected to decrease by 34% and 48%, respectively. Panels show the resulting percentage changes in the branching of ISOPO<sub>2</sub> between the NO and HO<sub>2</sub> oxidation channels, sulfate mass concentration, aerosol [H<sup>+</sup>] concentration, and isoprene SOA mass concentration. Values are summer means for the Southeast US boundary layer.